



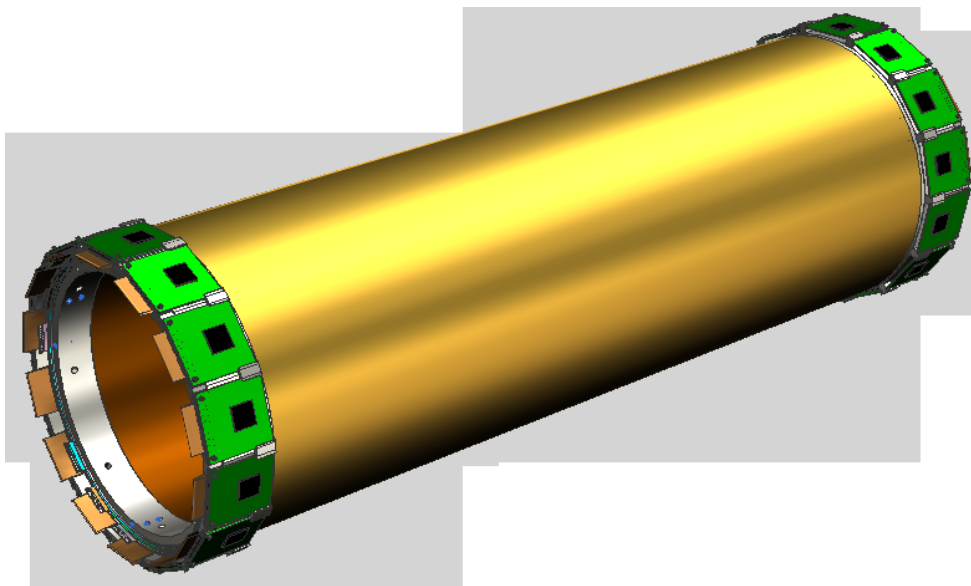
## Conceptual Design Report

# BESIII Cylindrical GEM Inner Tracker

BESIII Collaboration

July 3<sup>rd</sup>, 2014

Ver. 1.0.1



**Cover picture:** 3D view for the middle layer of the CGEM-IT.

# The BESIII Collaboration

M. Ablikim<sup>1</sup>, M. N. Achasov<sup>8,a</sup>, X. C. Ai<sup>1</sup>, O. Albayrak<sup>4</sup>, M. Albrecht<sup>3</sup>, D. J. Ambrose<sup>42</sup>, A. Amoroso<sup>46A,46C</sup>,  
 F. F. An<sup>1</sup>, Q. An<sup>43</sup>, F. Astorino<sup>46A</sup>, J. Z. Bai<sup>1</sup>, R. Baldini Ferroli<sup>19A</sup>, Y. Ban<sup>29</sup>, D. W. Bennett<sup>18</sup>,  
 J. V. Bennett<sup>18</sup>, M. Bertani<sup>19A</sup>, D. Bettoni<sup>20A</sup>, J. M. Bian<sup>41</sup>, F. Bianchi<sup>46A,46C</sup>, E. Boger<sup>22,g</sup>, O. Bondarenko<sup>23</sup>,  
 I. Boyko<sup>22</sup>, S. Braun<sup>38</sup>, R. A. Briere<sup>4</sup>, H. Cai<sup>48</sup>, X. Cai<sup>1</sup>, O. Cakir<sup>37A</sup>, A. Calcaterra<sup>19A</sup>, G. F. Cao<sup>1</sup>,  
 V. Carassiti<sup>20A</sup>, S. A. Cetin<sup>37B</sup>, J. F. Chang<sup>1</sup>, G. Chelkov<sup>22,b</sup>, G. Chen<sup>1</sup>, H. S. Chen<sup>1</sup>, J. C. Chen<sup>1</sup>,  
 M. L. Chen<sup>1</sup>, S. J. Chen<sup>27</sup>, X. Chen<sup>1</sup>, X. R. Chen<sup>24</sup>, Y. B. Chen<sup>1</sup>, H. P. Cheng<sup>16</sup>, X. K. Chu<sup>29</sup>, Y. P. Chu<sup>1</sup>,  
 G. Cibinetto<sup>20A</sup>, G. Cotto<sup>46A,46C</sup>, D. Cronin-Hennessy<sup>41</sup>, H. L. Dai<sup>1</sup>, J. P. Dai<sup>1</sup>, D. Dedovich<sup>22</sup>, Z. Y. Deng<sup>1</sup>,  
 A. Denig<sup>21</sup>, I. Denysenko<sup>22</sup>, M. Destefanis<sup>46A,46C</sup>, F. De Mori<sup>46A,46C</sup>, W. M. Ding<sup>31</sup>, Y. Ding<sup>25</sup>, C. Dong<sup>28</sup>,  
 J. Dong<sup>1</sup>, L. Y. Dong<sup>1</sup>, M. Y. Dong<sup>1</sup>, S. X. Du<sup>50</sup>, J. Z. Fan<sup>36</sup>, J. Fang<sup>1</sup>, S. S. Fang<sup>1</sup>, Y. Fang<sup>1</sup>,  
 R. Farinelli<sup>20A,20B</sup>, L. Fava<sup>46B,46C</sup>, G. Felici<sup>19A</sup>, C. Q. Feng<sup>43</sup>, E. Fioravanti<sup>20A</sup>, C. D. Fu<sup>1</sup>, O. Fuks<sup>22,g</sup>,  
 Q. Gao<sup>1</sup>, Y. Gao<sup>36</sup>, I. Garzia<sup>20A</sup>, C. Geng<sup>43</sup>, K. Goetzen<sup>9</sup>, W. X. Gong<sup>1</sup>, W. Gradl<sup>21</sup>, M. Greco<sup>46A,46C</sup>,  
 M. H. Gu<sup>1</sup>, Y. T. Gu<sup>11</sup>, Y. H. Guan<sup>1</sup>, L. B. Guo<sup>26</sup>, T. Guo<sup>26</sup>, Y. P. Guo<sup>21</sup>, Z. Haddadi<sup>23</sup>, S. Han<sup>48</sup>, Y. L. Han<sup>1</sup>,  
 F. A. Harris<sup>40</sup>, K. L. He<sup>1</sup>, M. He<sup>1</sup>, Z. Y. He<sup>28</sup>, T. Held<sup>3</sup>, Y. K. Heng<sup>1</sup>, Z. L. Hou<sup>1</sup>, C. Hu<sup>26</sup>, H. M. Hu<sup>1</sup>,  
 J. F. Hu<sup>46A</sup>, T. Hu<sup>1</sup>, G. M. Huang<sup>5</sup>, G. S. Huang<sup>43</sup>, H. P. Huang<sup>48</sup>, J. S. Huang<sup>14</sup>, L. Huang<sup>1</sup>, X. T. Huang<sup>31</sup>,  
 Y. Huang<sup>27</sup>, T. Hussain<sup>45</sup>, C. S. Ji<sup>43</sup>, Q. Ji<sup>1</sup>, P. Ji<sup>28</sup>, X. B. Ji<sup>1</sup>, X. L. Ji<sup>1</sup>, L. L. Jiang<sup>1</sup>, L. W. Jiang<sup>48</sup>,  
 X. S. Jiang<sup>1</sup>, J. B. Jiao<sup>31</sup>, Z. Jiao<sup>16</sup>, D. P. Jin<sup>1</sup>, S. Jin<sup>1</sup>, T. Johansson<sup>47</sup>, A. Julin<sup>41</sup>, N. Kalantar-Nayestanaki<sup>23</sup>,  
 X. L. Kang<sup>1</sup>, X. S. Kang<sup>28</sup>, M. Kavatsyuk<sup>23</sup>, B. C. Ke<sup>4</sup>, B. Kloss<sup>21</sup>, B. Kopf<sup>3</sup>, M. Kornicer<sup>40</sup>, W. Kuehn<sup>38</sup>,  
 A. Kupsc<sup>47</sup>, W. Lai<sup>1</sup>, J. S. Lange<sup>38</sup>, M. Lara<sup>18</sup>, P. Larin<sup>13</sup>, M. Leyhe<sup>3</sup>, C. H. Li<sup>1</sup>, Cheng Li<sup>43</sup>, Cui Li<sup>43</sup>, D. Li<sup>17</sup>,  
 D. M. Li<sup>50</sup>, F. Li<sup>1</sup>, G. Li<sup>1</sup>, H. B. Li<sup>1</sup>, J. C. Li<sup>1</sup>, Jin Li<sup>30</sup>, K. Li<sup>31</sup>, K. Li<sup>12</sup>, P. R. Li<sup>39</sup>, Q. J. Li<sup>1</sup>, T. Li<sup>31</sup>,  
 W. D. Li<sup>1</sup>, W. G. Li<sup>1</sup>, X. L. Li<sup>31</sup>, X. N. Li<sup>1</sup>, X. Q. Li<sup>28</sup>, Z. B. Li<sup>35</sup>, H. Liang<sup>43</sup>, Y. F. Liang<sup>33</sup>, Y. T. Liang<sup>38</sup>,  
 D. X. Lin<sup>13</sup>, B. J. Liu<sup>1</sup>, C. L. Liu<sup>4</sup>, C. X. Liu<sup>1</sup>, F. H. Liu<sup>32</sup>, Fang Liu<sup>1</sup>, Feng Liu<sup>5</sup>, H. B. Liu<sup>11</sup>, H. H. Liu<sup>15</sup>,  
 H. M. Liu<sup>1</sup>, J. Liu<sup>1</sup>, J. P. Liu<sup>48</sup>, K. Liu<sup>36</sup>, K. Y. Liu<sup>25</sup>, P. L. Liu<sup>31</sup>, Q. Liu<sup>39</sup>, S. B. Liu<sup>43</sup>, X. Liu<sup>24</sup>, Y. B. Liu<sup>28</sup>,  
 Z. A. Liu<sup>1</sup>, Zhiqiang Liu<sup>1</sup>, Zhiqing Liu<sup>21</sup>, H. Loehner<sup>23</sup>, X. C. Lou<sup>1,d</sup>, G. R. Lu<sup>14</sup>, H. J. Lu<sup>16</sup>, H. L. Lu<sup>1</sup>,  
 J. G. Lu<sup>1</sup>, Y. Lu<sup>1</sup>, Y. P. Lu<sup>1</sup>, C. L. Luo<sup>26</sup>, M. X. Luo<sup>49</sup>, T. Luo<sup>40</sup>, X. L. Luo<sup>1</sup>, M. Lv<sup>1</sup>, X. R. Lyu<sup>39</sup>, F. C. Ma<sup>25</sup>,  
 H. L. Ma<sup>1</sup>, Q. M. Ma<sup>1</sup>, S. Ma<sup>1</sup>, T. Ma<sup>1</sup>, X. Y. Ma<sup>1</sup>, F. E. Maas<sup>13</sup>, M. Maggiora<sup>46A,46C</sup>, Q. A. Malik<sup>45</sup>,  
 Y. J. Mao<sup>29</sup>, Z. P. Mao<sup>1</sup>, G. Maniscalco<sup>46A,46C</sup>, S. Marcello<sup>46A,46C</sup>, M. Melchiorri<sup>20A</sup>, J. G. Messchendorp<sup>23</sup>,  
 G. Mezzadri<sup>46A,46C</sup>, J. Min<sup>1</sup>, T. J. Min<sup>1</sup>, R. E. Mitchell<sup>18</sup>, X. H. Mo<sup>1</sup>, Y. J. Mo<sup>5</sup>, H. Moein<sup>23</sup>, C. Morales  
 Morales<sup>13</sup>, K. Moriya<sup>18</sup>, N. Yu. Muchnoi<sup>8,a</sup>, H. Muramatsu<sup>41</sup>, Y. Nefedov<sup>22</sup>, F. Nerling<sup>13</sup>, I. B. Nikolaev<sup>8,a</sup>,  
 Z. Ning<sup>1</sup>, S. Nisar<sup>7</sup>, X. Y. Niu<sup>1</sup>, S. L. Olsen<sup>30</sup>, Q. Ouyang<sup>1</sup>, S. Pacetti<sup>19B</sup>, P. Patteri<sup>19A</sup>, M. Pelizaeus<sup>3</sup>,  
 H. P. Peng<sup>43</sup>, K. Peters<sup>9</sup>, J. L. Ping<sup>26</sup>, R. G. Ping<sup>1</sup>, R. Poling<sup>41</sup>, M. Qi<sup>27</sup>, S. Qian<sup>1</sup>, C. F. Qiao<sup>39</sup>, L. Q. Qin<sup>31</sup>,  
 N. Qin<sup>48</sup>, X. S. Qin<sup>1</sup>, Y. Qin<sup>29</sup>, Z. H. Qin<sup>1</sup>, J. F. Qiu<sup>1</sup>, K. H. Rashid<sup>45</sup>, C. F. Redmer<sup>21</sup>, L. Rinchiuso<sup>20B</sup>,  
 M. Ripka<sup>21</sup>, A. Rivetti<sup>46C</sup>, G. Rong<sup>1</sup>, X. D. Ruan<sup>11</sup>, V. Santoro<sup>20A</sup>, A. Sarantsev<sup>22,e</sup>, M. Savrie<sup>20A,20B</sup>,  
 K. Schoenning<sup>47</sup>, S. Schumann<sup>21</sup>, W. Shan<sup>29</sup>, M. Shao<sup>43</sup>, C. P. Shen<sup>2</sup>, X. Y. Shen<sup>1</sup>, H. Y. Sheng<sup>1</sup>,  
 M. R. Shepherd<sup>18</sup>, W. M. Song<sup>1</sup>, X. Y. Song<sup>1</sup>, S. Sosio<sup>46A,46C</sup>, S. Spataro<sup>46A,46C</sup>, B. Spruck<sup>38</sup>, G. X. Sun<sup>1</sup>,  
 J. F. Sun<sup>14</sup>, S. S. Sun<sup>1</sup>, Y. J. Sun<sup>43</sup>, Y. Z. Sun<sup>1</sup>, Z. J. Sun<sup>1</sup>, Z. T. Sun<sup>43</sup>, C. J. Tang<sup>33</sup>, X. Tang<sup>1</sup>, I. Tapan<sup>37C</sup>,  
 E. H. Thorndike<sup>42</sup>, M. Tiemens<sup>23</sup>, D. Toth<sup>41</sup>, M. Ullrich<sup>38</sup>, I. Uman<sup>37B</sup>, G. S. Varner<sup>40</sup>, B. Wang<sup>28</sup>, D. Wang<sup>29</sup>,  
 D. Y. Wang<sup>29</sup>, K. Wang<sup>1</sup>, L. L. Wang<sup>1</sup>, L. S. Wang<sup>1</sup>, M. Wang<sup>31</sup>, P. Wang<sup>1</sup>, P. L. Wang<sup>1</sup>, Q. J. Wang<sup>1</sup>,  
 S. G. Wang<sup>29</sup>, W. Wang<sup>1</sup>, X. F. Wang<sup>36</sup>, Y. D. Wang<sup>19A</sup>, Y. F. Wang<sup>1</sup>, Y. Q. Wang<sup>21</sup>, Z. Wang<sup>1</sup>, Z. G. Wang<sup>1</sup>,  
 Z. H. Wang<sup>43</sup>, Z. Y. Wang<sup>1</sup>, D. H. Wei<sup>10</sup>, J. B. Wei<sup>29</sup>, P. Weidenkaff<sup>21</sup>, S. P. Wen<sup>1</sup>, M. Werner<sup>38</sup>, U. Wiedner<sup>3</sup>,  
 M. Wolke<sup>47</sup>, L. H. Wu<sup>1</sup>, N. Wu<sup>1</sup>, Z. Wu<sup>1</sup>, L. G. Xia<sup>36</sup>, Y. Xia<sup>17</sup>, D. Xiao<sup>1</sup>, Z. J. Xiao<sup>26</sup>, Y. G. Xie<sup>1</sup>, Q. L. Xiu<sup>1</sup>,  
 G. F. Xu<sup>1</sup>, L. Xu<sup>1</sup>, Q. J. Xu<sup>12</sup>, Q. N. Xu<sup>39</sup>, X. P. Xu<sup>34</sup>, Z. Xue<sup>1</sup>, L. Yan<sup>43</sup>, W. B. Yan<sup>43</sup>, W. C. Yan<sup>43</sup>,  
 Y. H. Yan<sup>17</sup>, H. X. Yang<sup>1</sup>, L. Yang<sup>48</sup>, Y. Yang<sup>5</sup>, Y. X. Yang<sup>10</sup>, H. Ye<sup>1</sup>, M. Ye<sup>1</sup>, M. H. Ye<sup>6</sup>, B. X. Yu<sup>1</sup>,  
 C. X. Yu<sup>28</sup>, H. W. Yu<sup>29</sup>, J. S. Yu<sup>24</sup>, S. P. Yu<sup>31</sup>, C. Z. Yuan<sup>1</sup>, W. L. Yuan<sup>27</sup>, Y. Yuan<sup>1</sup>, A. Yuncu<sup>37B,f</sup>,  
 A. A. Zafar<sup>45</sup>, A. Zallo<sup>19A</sup>, S. L. Zang<sup>27</sup>, Y. Zeng<sup>17</sup>, B. X. Zhang<sup>1</sup>, B. Y. Zhang<sup>1</sup>, C. Zhang<sup>27</sup>, C. B. Zhang<sup>17</sup>,  
 C. C. Zhang<sup>1</sup>, D. H. Zhang<sup>1</sup>, H. H. Zhang<sup>35</sup>, H. Y. Zhang<sup>1</sup>, J. J. Zhang<sup>1</sup>, J. Q. Zhang<sup>1</sup>, J. W. Zhang<sup>1</sup>,  
 J. Y. Zhang<sup>1</sup>, J. Z. Zhang<sup>1</sup>, S. H. Zhang<sup>1</sup>, X. J. Zhang<sup>1</sup>, X. Y. Zhang<sup>31</sup>, Y. Zhang<sup>1</sup>, Y. H. Zhang<sup>1</sup>, Z. H. Zhang<sup>5</sup>,  
 Z. P. Zhang<sup>43</sup>, Z. Y. Zhang<sup>48</sup>, G. Zhao<sup>1</sup>, J. W. Zhao<sup>1</sup>, Lei Zhao<sup>43</sup>, Ling Zhao<sup>1</sup>, M. G. Zhao<sup>28</sup>, Q. Zhao<sup>1</sup>,  
 Q. W. Zhao<sup>1</sup>, S. J. Zhao<sup>50</sup>, T. C. Zhao<sup>1</sup>, X. H. Zhao<sup>27</sup>, Y. B. Zhao<sup>1</sup>, Z. G. Zhao<sup>43</sup>, A. Zhemchugov<sup>22,g</sup>,  
 B. Zheng<sup>44</sup>, J. P. Zheng<sup>1</sup>, Y. H. Zheng<sup>39</sup>, B. Zhong<sup>26</sup>, L. Zhou<sup>1</sup>, Li Zhou<sup>28</sup>, X. Zhou<sup>48</sup>, X. K. Zhou<sup>39</sup>,  
 X. R. Zhou<sup>43</sup>, X. Y. Zhou<sup>1</sup>, K. J. Zhu<sup>1</sup>, X. L. Zhu<sup>36</sup>, Y. C. Zhu<sup>43</sup>, Y. S. Zhu<sup>1</sup>, Z. A. Zhu<sup>1</sup>, J. Zhuang<sup>1</sup>,  
 L. Zotti<sup>46A,46C</sup>, B. S. Zou<sup>1</sup>, J. H. Zou<sup>1</sup>

(BESIII Collaboration)

<sup>1</sup> Institute of High Energy Physics, Beijing 100049, People's Republic of China

<sup>2</sup> Beihang University, Beijing 100191, People's Republic of China

- <sup>3</sup> Bochum Ruhr-University, D-44780 Bochum, Germany
- <sup>4</sup> Carnegie Mellon University, Pittsburgh, Pennsylvania 15213, USA
- <sup>5</sup> Central China Normal University, Wuhan 430079, People's Republic of China
- <sup>6</sup> China Center of Advanced Science and Technology, Beijing 100190, People's Republic of China
- <sup>7</sup> COMSATS Institute of Information Technology, Lahore, Defence Road, Off Raiwind Road, 54000 Lahore, Pakistan
- <sup>8</sup> G.I. Budker Institute of Nuclear Physics SB RAS (BINP), Novosibirsk 630090, Russia
- <sup>9</sup> GSI Helmholtzcentre for Heavy Ion Research GmbH, D-64291 Darmstadt, Germany
- <sup>10</sup> Guangxi Normal University, Guilin 541004, People's Republic of China
- <sup>11</sup> GuangXi University, Nanning 530004, People's Republic of China
- <sup>12</sup> Hangzhou Normal University, Hangzhou 310036, People's Republic of China
- <sup>13</sup> Helmholtz Institute Mainz, Johann-Joachim-Becher-Weg 45, D-55099 Mainz, Germany
- <sup>14</sup> Henan Normal University, Xinxiang 453007, People's Republic of China
- <sup>15</sup> Henan University of Science and Technology, Luoyang 471003, People's Republic of China
- <sup>16</sup> Huangshan College, Huangshan 245000, People's Republic of China
- <sup>17</sup> Hunan University, Changsha 410082, People's Republic of China
- <sup>18</sup> Indiana University, Bloomington, Indiana 47405, USA
- <sup>19</sup> (A)INFN Laboratori Nazionali di Frascati, I-00044, Frascati, Italy; (B)INFN and University of Perugia, I-06100, Perugia, Italy
- <sup>20</sup> (A)INFN Sezione di Ferrara, I-44122, Ferrara, Italy; (B)University of Ferrara, I-44122, Ferrara, Italy
- <sup>21</sup> Johannes Gutenberg University of Mainz, Johann-Joachim-Becher-Weg 45, D-55099 Mainz, Germany
- <sup>22</sup> Joint Institute for Nuclear Research, 141980 Dubna, Moscow region, Russia
- <sup>23</sup> KVI, University of Groningen, NL-9747 AA Groningen, The Netherlands
- <sup>24</sup> Lanzhou University, Lanzhou 730000, People's Republic of China
- <sup>25</sup> Liaoning University, Shenyang 110036, People's Republic of China
- <sup>26</sup> Nanjing Normal University, Nanjing 210023, People's Republic of China
- <sup>27</sup> Nanjing University, Nanjing 210093, People's Republic of China
- <sup>28</sup> Nankai University, Tianjin 300071, People's Republic of China
- <sup>29</sup> Peking University, Beijing 100871, People's Republic of China
- <sup>30</sup> Seoul National University, Seoul, 151-747 Korea
- <sup>31</sup> Shandong University, Jinan 250100, People's Republic of China
- <sup>32</sup> Shanxi University, Taiyuan 030006, People's Republic of China
- <sup>33</sup> Sichuan University, Chengdu 610064, People's Republic of China
- <sup>34</sup> Soochow University, Suzhou 215006, People's Republic of China
- <sup>35</sup> Sun Yat-Sen University, Guangzhou 510275, People's Republic of China
- <sup>36</sup> Tsinghua University, Beijing 100084, People's Republic of China
- <sup>37</sup> (A)Ankara University, Dogol Caddesi, 06100 Tandogan, Ankara, Turkey; (B)Dogus University, 34722 Istanbul, Turkey; (C)Uludag University, 16059 Bursa, Turkey
- <sup>38</sup> Universitaet Giessen, D-35392 Giessen, Germany
- <sup>39</sup> University of Chinese Academy of Sciences, Beijing 100049, People's Republic of China
- <sup>40</sup> University of Hawaii, Honolulu, Hawaii 96822, USA
- <sup>41</sup> University of Minnesota, Minneapolis, Minnesota 55455, USA
- <sup>42</sup> University of Rochester, Rochester, New York 14627, USA
- <sup>43</sup> University of Science and Technology of China, Hefei 230026, People's Republic of China
- <sup>44</sup> University of South China, Hengyang 421001, People's Republic of China
- <sup>45</sup> University of the Punjab, Lahore-54590, Pakistan
- <sup>46</sup> (A)University of Turin, I-10125, Turin, Italy; (B)University of Eastern Piedmont, I-15121, Alessandria, Italy; (C)INFN, I-10125, Turin, Italy
- <sup>47</sup> Uppsala University, Box 516, SE-75120 Uppsala, Sweden
- <sup>48</sup> Wuhan University, Wuhan 430072, People's Republic of China
- <sup>49</sup> Zhejiang University, Hangzhou 310027, People's Republic of China
- <sup>50</sup> Zhengzhou University, Zhengzhou 450001, People's Republic of China
- <sup>a</sup> Also at the Novosibirsk State University, Novosibirsk, 630090, Russia
- <sup>b</sup> Also at the Moscow Institute of Physics and Technology, Moscow 141700, Russia and at the Functional Electronics Laboratory, Tomsk State University, Tomsk, 634050, Russia
- <sup>c</sup> Currently at Arel University, Kucukcekmece, Istanbul, Turkey
- <sup>d</sup> Also at University of Texas at Dallas, Richardson, Texas 75083, USA
- <sup>e</sup> Also at the PNPI, Gatchina 188300, Russia
- <sup>f</sup> Also at Bogazici University, 34342 Istanbul, Turkey
- <sup>g</sup> Also at the Moscow Institute of Physics and Technology, Moscow 141700, Russia

---

Editors:	R. Baldini	Email: rinaldo.baldini@centrofermi.it
	M. Bertani	Email: monica.bertani@lnf.infn.it
	F. Bianchi	Email: fabrizio.bianchi@to.infn.it
	A. Calcaterra	Email: alessandro.calcaterra@lnf.infn.it
	G. Cibinetto	Email: cibinetto@fe.infn.it
	M. Destefanis	Email: marco.destefanis@to.infn.it
	M. Dong	Email: dongmy@mail.ihep.ac.cn
	G. Felici	Email: giulietto.felici@lnf.infn.it
	X. Ji	Email: jixl@ihep.ac.cn
	T. Johansson	Email: tord.johansson@physics.uu.se
	Z. Liu	Email: liuza@ihep.ac.cn
	M. Maggiora	Email: marco.maggiora@to.infn.it
	S. Marcello	Email: marcello@to.infn.it
	P. Marciniewski	Email: pawel.marciniewski@fysast.uu.se
	Q. Ouyang	Email: ouyq@ihep.ac.cn
	A. Rivetti	Email: rivetti@to.infn.it
	C. Rosner	Email: chrosner@students.uni-mainz.de
	M. Savrié	Email: savrie@fe.infn.it
	S. Spataro	Email: spataro@to.infn.it
	K. Wang	Email: wangk@ihep.ac.cn
	L. Wang	Email: llwang@ihep.ac.cn
	L. Wu	Email: wulh@ihep.ac.cn
	M. Ye	Email: yem@ihep.ac.cn
	Y. Zhang	Email: yao.zhang@ihep.ac.cn
Spokesperson:	Xiaoyan Shen	Email: shenxy@ihep.ac.cn
Co-Spokespersons:	Wolfgang Gradl	Email: wgradl@slac.stanford.edu
	Yangheng Zheng	Email: zhengyh@gucas.ac.cn

---



## Preface

The BESIII spectrometer and the BEPCII  $e^+e^-$  collider offer an unique experimental setup to investigate Particle Physics.

The excellent performances of the spectrometer and the unprecedented luminosities of BEPCII have already allowed to collect in the last few years world record statistics at different center of mass energies in the Charmonium and Open Charm mass range, and more will come in the next years. BESIII is in fact expected to take data until at least 2022 and more likely until 2024.

Due to the very high BEPCII luminosities, the current Inner Tracker of the BESIII spectrometer, a drift chamber, is starting to show aging effects that in few years will affect significantly the detector performances. A possible solution would be to build a new Inner Tracker composed of Cylindrical Gas Electron Multiplier (CGEM) detectors.

The present document describes the conceptual design of such a CGEM Inner Tracker (CGEM-IT), and in particular:

- the design and construction of a prototype that will constitute one of the layers of the CGEM-IT;
- the key innovations, as the new Rohacell supports and an innovative anode design, that will make the BESIII CGEM-IT a new kind of detector;
- the efforts devoted to develop and test a software framework in order to simulate and reconstruct the CGEM-IT data;
- possible benchmark channels that could be investigated in the near future once the software framework will be more mature;
- those activities related to the design and construction of a suitable Front End Electronics;
- the Financial Plan and the Community that has aggregated within the BESIII Collaboration to build the CGEM-IT.

---

The use of registered names, trademarks, *etc.* in this publication does not imply, even in the absence of specific statement, that such names are exempt from the relevant laws and regulations and therefore free for general use.

# Contents

---

<b>Preface</b>	<b>vii</b>	4.4 Off-Detector Electronics . . . . .	23
<b>1 Introduction</b>	<b>1</b>	4.4.1 Readout Boards . . . . .	23
1.1 The Present BESIII Inner Tracker . .	2	4.4.2 Concentrator Boards . . . . .	24
1.2 Present and Expected Backgrounds .	3	<b>5 DAQ and Trigger</b>	<b>25</b>
1.3 Inner Tracker Upgrade Requirements	5	5.1 Requirements . . . . .	25
<b>2 Detector Design</b>	<b>7</b>	5.2 Bandwidth . . . . .	25
2.1 Operating Principle of a Triple Cylindrical GEM Detector . . . . .	7	5.3 Storage . . . . .	25
2.1.1 The KLOE-2 Inner Tracker: Know-How and status . . . . .	7	<b>6 Integration of the CGEM-IT with the Spectrometer</b>	<b>27</b>
2.2 BESIII CGEM Innovations . . . . .	7	6.1 Interfacing Mechanical Design . . . . .	27
2.2.1 Rohacell . . . . .	8	6.2 HV Systems . . . . .	27
2.2.2 Anode design . . . . .	8	6.2.1 Requirements . . . . .	27
2.2.3 Analog vs Digital Readout . . . . .	9	6.2.2 Overall Design . . . . .	27
2.2.4 Planar Test Setup . . . . .	9	6.2.3 Connectors and cables . . . . .	28
<b>3 The BESIII CGEM-IT</b>	<b>13</b>	6.2.4 Distribution Boxes . . . . .	28
3.1 CGEM-IT vs DC-IT . . . . .	13	6.2.5 HV summary . . . . .	29
3.2 Mechanical Design . . . . .	14	6.3 Slow Controls . . . . .	29
3.2.1 Construction Technique . . . . .	14	<b>7 Simulation of Cylindrical GEM Inner Tracker</b>	<b>31</b>
3.2.2 Detector Components . . . . .	15	7.1 Parametric Simulations . . . . .	31
3.2.3 Material Budget . . . . .	16	7.1.1 Digitization and Cluster Model . .	31
3.3 Tooling and Construction . . . . .	16	7.2 CGEM-IT Full Offline Reconstruction	32
3.3.1 Quality Controls and preliminary operations . . . . .	16	7.2.1 Cluster Reconstruction for CGEM	32
3.3.2 Obtaining cylindrical GEM and electrode foils . . . . .	17	7.2.2 Track finding with the Drift-Chamber-Outer-Tracker . . . . .	33
<b>4 Front End Electronics</b>	<b>19</b>	7.2.3 Track fitting . . . . .	34
4.1 Requirements . . . . .	19	7.3 Monte Carlo Simulation . . . . .	34
4.1.1 Time resolution . . . . .	19	<b>8 Tasks and Plans</b>	<b>37</b>
4.1.2 Dead Time Estimation . . . . .	19	8.1 Tasks . . . . .	37
4.2 System Block Description . . . . .	19	8.1.1 CGEM-IT design . . . . .	37
4.3 On-Detector Electronics . . . . .	20	8.1.2 CGEM-IT construction . . . . .	38
4.3.1 Charge Measurement Specifications	20	8.1.3 CGEM-IT electronics . . . . .	39
4.3.2 Time Measurement Specifications	21	8.1.4 CGEM-IT data simulation and analysis . . . . .	41
4.3.3 Preamplifier Boards . . . . .	21	8.1.5 CGEM-IT DAQ and Trigger . . .	42
4.3.4 The front-end ASIC . . . . .	22	8.2 Schedule . . . . .	42

8.3	Manpower . . . . .	42
8.4	Financial issues . . . . .	44
8.4.1	Direct Funding . . . . .	44
8.4.2	Indirect Funding . . . . .	44
<b>Acknowledgements</b>		<b>47</b>
<b>Acronyms</b>		<b>49</b>
<b>List of Figures</b>		<b>51</b>
<b>List of Tables</b>		<b>53</b>

# 1 Introduction

---

<b>COMMENT:</b>	<b>Author(s):</b>	<b>Maggiore, Bertani, Qun</b>
-----------------	-------------------	-----------------------------------

The Inner Tracker (IT) is a key detector in a Particle Physics spectrometer; excellent spatial and momentum resolutions, radiation hardness and high occupancy capability are its main requirements. The existing Inner Drift Chamber (denoted in this report as DC or MDC) of the Beijing Spectrometer III (BESIII) [?] is showing aging effects due to the very high luminosities of the Beijing electron positron collider II (BEPCII), a high luminosity, multi-bunch  $e^+ e^-$  collider running at center of mass energies in the tau-charm region [?]. To solve this problem, we propose to design, construct and, upon approval by the BESIII Collaboration, deploy and commission by the end of 2017 an Inner Tracker (IT) to be inserted inside the existing Outer Drift Chamber.

Such a new IT should be characterised by a significant radiation hardness, high rate capability, excellent resolutions both in the longitudinal and transverse directions, a good time resolution, and a limited total radiation length; the space available in the inner part of the BESIII spectrometer is quite limited, and this introduces significant constraints on the mechanical design and on the power dissipation per readout channel.

Gas Electron Multiplier (GEM) detectors offer an ideal technique to address the above described requirements. Very recently a new photolithographic process (the so called single-mask technology [?]) has overcome those limitations of the original double-mask technology that prevents its use in large-size detectors, and has been proven to be mature in the last few years on small and large-size detectors [?]. The single-mask GEM sheets that will be used to build the new IT, with a sheet width up to 550 mm, are among the widest ones installed up to now in detectors not dedicated to R&D.

GEM sheets are usually adopted to assemble planar detectors; but a cylindrically symmetric detector would be a perfect and innovative IT for a spectrometer hosted on a symmetric collider. Only one single Cylindrical-GEM (CGEM) based detector has been built up to now, by the KLOE-2 Collaboration [?, ?], and it is currently in its commissioning stage [?]. The path paved by the KLOE-2 Collaboration allows the construction of the CGEM-IT not starting from scratch: several of the people in-

involved from INFN, IHEP and Uppsala did participate to the design and construction of the KLOE-2 CGEM-IT or of its electronics, and constitute a valuable knowledge base to replicate the solutions introduced by KLOE-2 and to further proceed introducing other new innovative aspects in the design and construction of the BESIII CGEM-IT.

We aim to build a three-layer CGEM-IT that will fulfill the requirements quoted above. Among them, a limited total radiation length is essential to provide effective tracking and a global good spatial and momentum resolution. We plan to introduce a significant innovation w.r.t. the state of the art of GEM detectors, and w.r.t. the KLOE-2 CGEM-IT as well: building supports for the sub-layers composed of Rohacell instead of the standard Honeycomb allow to significantly reduce the total radiation length of the detector, down to almost 60% compared to an equivalent structure composed of Honeycomb. Colleagues from Ferrara possess the required knowledge, and have developed in their laboratories the proper mechanical techniques to produce such lighter but equally strong supports (see Chap. 3).

The support structure and hence the low total radiation length is not the only innovation. There is room for improvements in the readout design as well. An innovative design of the anode readout is currently under investigation, and could modify the capacitances of the anode w.r.t. the standard readout to obtain a cleaner signal (see Sec. 2.2.2).

The mechanical design of the first layer of the CGEM-IT has been already completed and thanks to the funds coming from the INFN-MAE-MOST Project (see Chap. 8.1) the corresponding material has been mostly already procured; its construction will start at Ferrara and LNF in late June 2014. Such a first layer will act as the prototype for the two other layers needed to assemble the full CGEM-IT.

A requirement among those cited above is an excellent spatial resolution: the goal for the CGEM-IT detector is an overall spatial resolution better than 100  $\mu\text{m}$ . The digital readout electronics developed for KLOE-2 does not fit this requirement of the BESIII CGEM-IT, since the required spatial resolution, in presence of the 1 Tesla magnetic field of the BESIII experiment, would impose a high segmentation and a prohibitive number of channels.

Therefore, an innovative readout based on analogue information and data pushing architecture will be developed (see Chap. 4). Analogue readout allows to identify the charge centroid with a moderate strip pitch, while data pushing architecture allows to move the overall apparatus readout synchronization to the off-line farms using the time-tag approach. Moreover, the GASTONE ASIC for the KLOE-2 CGEM-IT has been developed [?, ?] using AMS CMOS 0.35  $\mu\text{m}$  technology, which cannot be exported in the People's Republic of China (P.R.C.). Hence, a new analogue readout has to be designed in order to measure the charge centroid and to make over to a different technology, such as UMC 0.11  $\mu\text{m}$ , which can be exported in P.R.C..

The design and construction of the CGEM-IT detector has to be paired with the development of proper tracking algorithms and of custom simulation and reconstruction software. The new possibilities introduced by such a detector in reconstructing rare final states with a very precise determination of secondary vertices offer new possibilities to improve the reconstruction efficiency of such kind of events, and to increase the background rejection. The proper benchmark channels have to be identified, and detailed simulations have to be performed making use of state of the art techniques, in order to make the best possible use of the potential of this kind of detector. The very same software will allow to analyse the first data coming from the CGEM-IT immediately after its deployment in the existing BESIII spectrometer, and hence to support the commissioning of the new IT. The present status of the design, development and testing of such a dedicated software framework is discussed in Chap. 7, as those benchmark channels that could be investigated once the framework will reach in the next months a more mature stage.

Before proceeding to the description of the CGEM-IT design and building, an overview of the present experimental scenario is needed, in order to define the requirements and the constraints for the CGEM-IT construction.

## 1.1 The Present BESIII Inner Tracker

**COMMENT: Author(s): Mingyi DONG**

The main tracking detector of BESIII is a drift chamber (MDC), characterized by a low-mass cylindrical chamber with small-cell geometry, and a helium-based gas that operates in a 1T magnetic

field. MDC consists of an inner chamber and an outer chamber, which are joined together at the endplates, sharing a common gas volume [?]. The inner chamber was designed to be replaced in case of radiation damage.

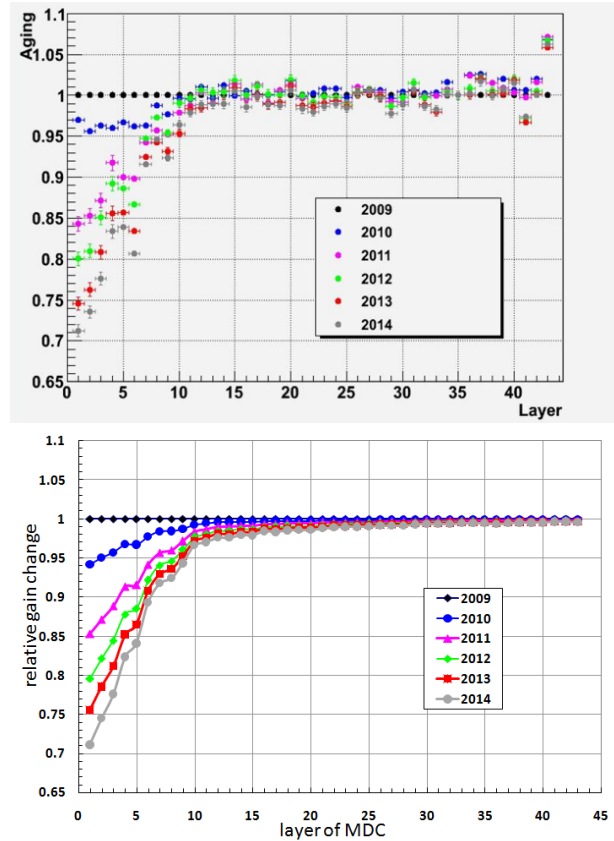


**Figure 1.1:** MDC gain changes in each year (the up is from Bhabha events, and the down is from accumulated charges with aging ration of 0.3% methods).

After five years of operation, the MDC inner chamber is suffering from aging problems due to a huge beam related background. The gains of the inner chamber experience an obvious decrease, reaching a maximum decline of about 29% for the first layer cells. Two calculation methods for the gains (Bhabha events and accumulated charges with 0.3% aging ratio) get almost the same results, shown in Fig. 1.1. In order to reduce the dark currents of the sense wires to protect the detector, the operation high voltages of the first four layers have to be set to 96%, 97%, 98% and 99% of the normal value respectively. This contributes to the decrease of the effective gain and leads to worse performance of the inner chamber. The present spatial resolution and hit efficiency of MDC are shown in Fig. 1.2.

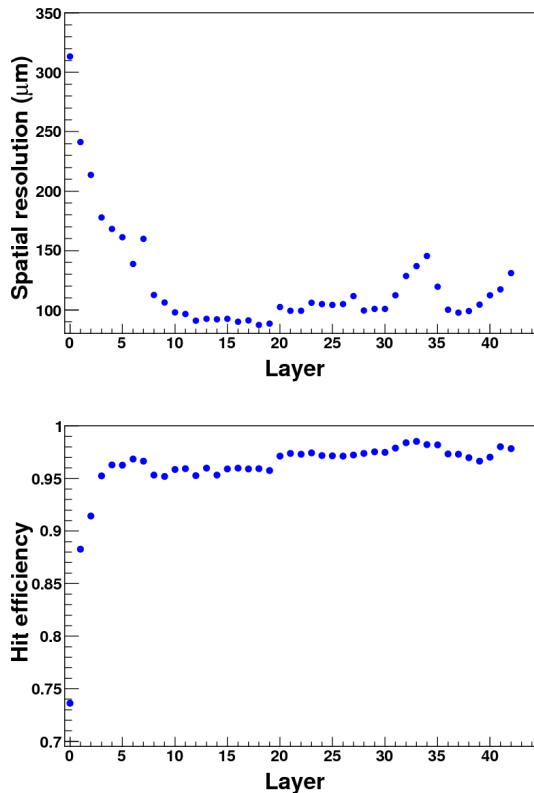


**Figure 1.2:** Spatial resolution (up) and hit efficiency (down) of each layer.

## 1.2 Present and Expected Backgrounds

**COMMENT: Author(s): Mingyi DONG, Gianluigi Cibinetto**

Experimental investigations show that the beam related backgrounds mostly come from the beam gas interaction and the Touschek effect, which depend on the machine status, especially at high beam currents.

The effect of background level can be extracted from measurement of the dark currents of MDC. The accumulated charges of each layer, obtained by integrating the dark currents in every year, are shown in Fig. 1.3. In the last two years the accumulated charges are smaller than before, about 14 mC/cm for the first year. This is due to the improvement of the machine status from 2009 to 2013, and then keep almost the same level from 2013 to 2014.

High backgrounds lead to high counting rates. Fig. 1.4 shows the counting rate of each MDC layer for two runs with different beam conditions. The count-

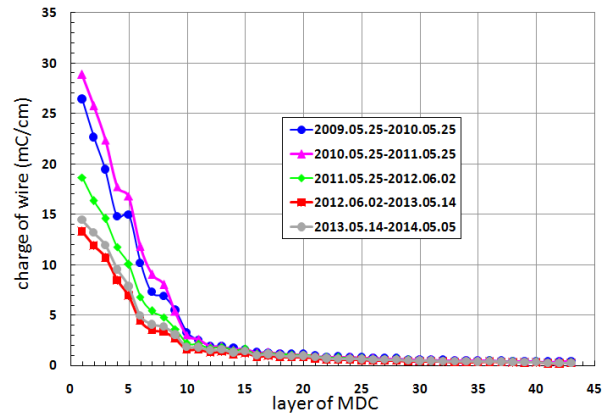


**Figure 1.3:** The accumulated charges of MDC in each year.

ing rate was about 110 kHz per sense wire for the first layer in 2012 (top plot), and reduces to about the half in 2014 (bottom plot). Those measurements have been obtained analyzing the first 30 s of random trigger data.

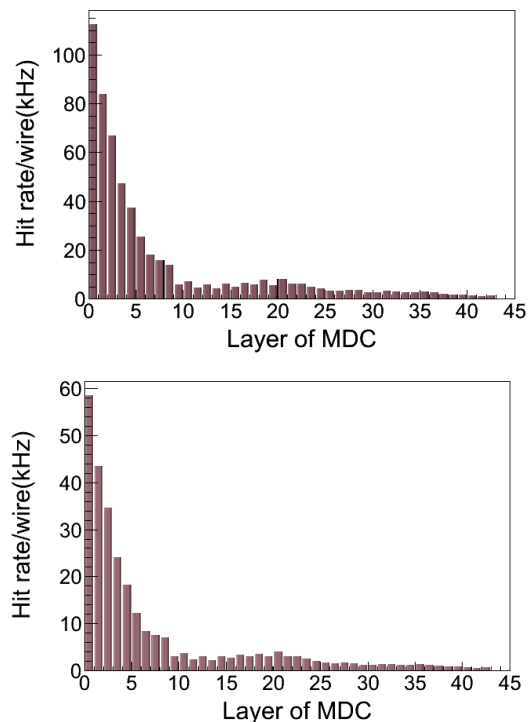


**Figure 1.4:** The counting rate of each MDC layer, extracted processing the first 30 s of random trigger data. Top plot represents a run from 2012 and bottom plot is a run from 2014.

Using an alternative method we extract the dark count rates averaged over a run. We analyze ran-

dom trigger events using the background mixing routine which add noise data to a fake Monte Carlo process, taking into account the luminosity curve. We obtain, for the same two runs processed with the other method, the distributions shown in Fig. 1.5. The rate values on the innermost layer of the drift chamber are, as expected, from 15% to 30% lower than the peak values estimated earlier.

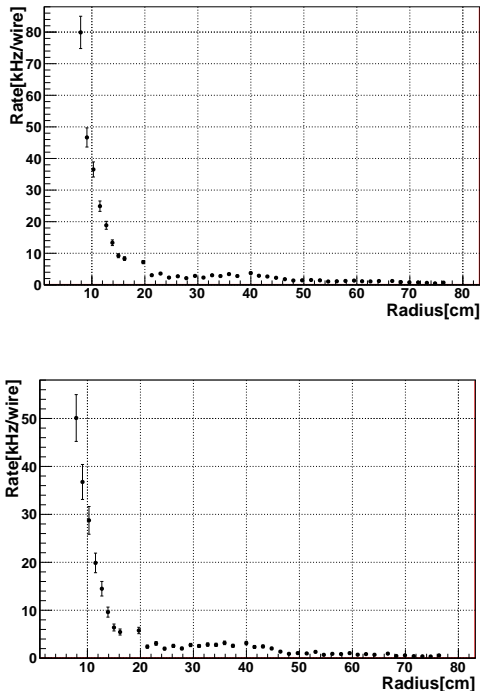


**Figure 1.5:** Average rate per wire on the inner drift chamber as function of the radius, calculated with background mixing procedure as described in the text. Each point represents a layer. The inner drift chamber is composed by the first eight layers. Top plot represents a run from 2012 and bottom plot is a run from 2014.

Since the background level is mainly related to machine conditions and beam parameters we calculated the average wire rate of the MDC innermost layer for runs belonging to different recent running periods (Fig. 1.6). We decide to use for our estimate the worst case, among the ones we analyzed, that is the run from 2012 having an average wire background level of 80 kHz which translates to a rate less than 1 kHz/cm<sup>2</sup>.

The expected background rate on the CGEM-IT can be estimated from combining the MDC background data with Monte Carlo (MC) simulations. MDC data are used to map the actual background level of the interaction region. Then the different geometry and material composition of the two de-

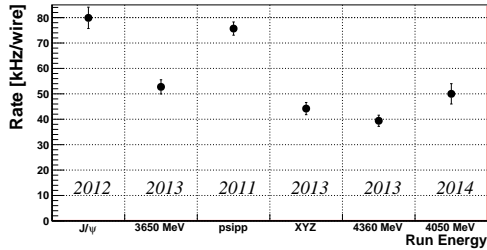


**Figure 1.6:** Average rate per wire on the first layer of the drift chamber for different running periods calculated with background mixing procedure.

tectors is taken into account using GEANT4 full simulation. Finally the expected strip rate for the CGEM-IT is computed as

$$R_{GEM}^{exp}(r) = R_{MDC}^{data}(r) \times \frac{R_{GEM}^{MC}(r)}{R_{MDC}^{MC}(r)} \quad (1.1)$$

where  $R_{GEM}^{exp}(r)$  is the expected rate per strip on the CGEM-IT as function of the radius ( $r$ ),  $R_{MDC}^{data}$  is the MDC wire rate measured from random trigger data, and  $R_{GEM}^{MC}$  and  $R_{MDC}^{MC}$  are the related quantities extracted from the MC simulation. If needed, interpolation is used to match the radii of the MDC layers and the CGEM planes. For the CGEM, only the X-strips, parallel to the beam direction, have been considered.

$e^+e^- \rightarrow n\gamma e^+e^-$  MC sample, produced with Bh-wide generator [?], has been used for this study. The use of this process is enough for our purpose since the MC is only used to scale the rates from MDC data to the different detector design. The effect of different angular distributions on the scale factor has been checked using different processes for which we found deviations less than 20%. The CGEM full simulation includes a preliminary digitization and takes into account the strip multiplicity. We used BOSS version 6.6.4.p01 with CGEM-0.0.2. A detailed description of the CGEM simulation is reported in Section 7.

Using the procedure described above we calculate the expected average rate per strip for each of the three CGEM-IT layers (see Fig. 1.7); for the innermost layer the average strip rate is expected to be about 9.5 kHz, that is some how consistent by scaling the MDC rate by the different strip/cell size and considering a CGEM strip multiplicity of 3. Assuming for the front-end electronics, a time window of 1  $\mu$ s (see 4.4), we estimate the average strip occupancy for the innermost layer, *i.e.* the probability for each trigger to find a strip fired, to be a little

less than 1%.

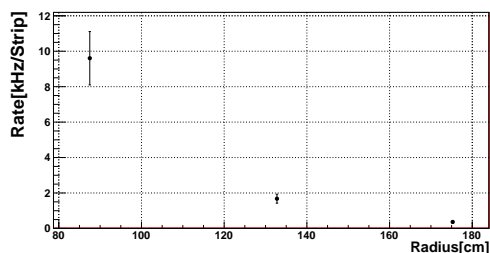


**Figure 1.7:** Expected average rate per X-strip on the CGEM-IT as function the radius.

Since these results are extracted directly from the MDC rates averaged over an entire run, we rescale the strip rate to the ratio peak/average MDC rate per wire of the innermost layer (in the worst case  $120[\text{kHz}]/80[\text{kHz}]$ ), obtaining 14 kHz/strip.

A safety factor  $\times 4$  has to be considered in order to take into account approximations in the detector description and digitization, systematic errors due to the angular distribution, high background running periods and luminosity increase. Therefore we can conclude that the maximum rate to be considered on the CGEM-IT is about 60 kHz per strip.

### 1.3 Inner Tracker Upgrade Requirements

**COMMENT: Author(s): Mingyi DONG**

If the backgrounds stay at the same level as the last two years, the gain of the MDC first layer will decrease about 4% each year according to the aging ratio of 0.3%, so we can estimate that the gain of the first layer will become 63% by 2016. It's of paramount importance to start planning for an upgrade if the BESIII inner tracker. To match the available space for inner tracker and meet the BESIII physical requirements, the upgrade of the inner drift chamber should take into account the following points:

- 1) the possible radial extension is from 59 mm to 183.5 mm, and the detector covers a polar angle of  $|\cos \vartheta| = 0.93$ ;
- 2) the spatial resolution has to be better than 120  $\mu\text{m}$  in  $r$ - $\varphi$  direction, and better than 1 mm in Z direction;
- 3) the material budget has to be less than 1.5%  $X_0$ ;

- 4) the detector has to work properly also at counting rate larger than 4 kHz/cm<sup>2</sup>.

## References

- [1] D.M. Asner, T. Barnes, J.M. Bian, I.I. Bigi, N. Brambilla, et al. Physics at BES-III. *Int.J.Mod.Phys.*, A24:S1–794, 2009.
- [2] BESIII Collaboration. Preliminary design report of the besiii detector. Technical report, 2004.
- [3] Serge Duarte Pinto, Marco Villa, Matteo Alfonsi, Ian Brock, Gabriele Croci, et al. Progress on large area GEMs. *JINST*, 4:P12009, 2009.
- [4] Marco Villa, Serge Duarte Pinto, Matteo Alfonsi, Ian Brock, Gabriele Croci, et al. Progress on large area GEMs. *Nucl.Instrum.Meth.*, A628:182–186, 2011.
- [5] A. Balla, G. Bencivenni, S. Cerioni, P. Ciambrone, E. De Lucia, et al. Status of the Cylindrical-GEM project for the KLOE-2 inner tracker. 2009.
- [6] A. Balla, G. Bencivenni, M. Capodiferro, S. Cerioni, P. Ciambrone, et al. A new cylindrical-GEM inner tracker for the upgrade of the KLOE experiment. *Nucl.Phys.Proc.Suppl.*, 215:76–78, 2011.
- [7] A. Balla, G. Bencivenni, P. Branchini, A. Budano, M. Capodiferro, et al. Production and test of the first two layers of the KLOE-2 Inner Tracker. *Nucl.Instrum.Meth.*, A718:416–417, 2013.
- [8] A. Balla, G. Bencivenni, M. Beretta, S. Cerioni, P. Ciambrone, et al. GASTONE: A new ASIC for the cylindrical GEM inner tracker of KLOE experiment at DAFNE. *Nucl.Instrum.Meth.*, A604:23–25, 2009.
- [9] A. Balla, G. Bencivenni, P. Branchini, A. Budano, S. Cerioni, et al. GASTONE64: A new front-end ASIC for the cylindrical GEM Inner Tracker of KLOE-2 experiment at *DAΦFNE*. *Nucl.Instrum.Meth.*, A732:523–525, 2013.
- [10] C. Chen et al. The BESIII drift chamber. *IEEE Nuclear Science Symposium Conference Record 2007, NSS 07*, 3:1844–1846, 2007.
- [11] <http://docbes3.ihep.ac.cn/offlinesoftware/index.php/Generator>.



## 2 Detector Design

**COMMENT: Author(s): Cibinetto, Calcaterra**

The new Inner Tracker will be installed in the available space left by the removal of the Inner Drift Chamber. The proposed solution consists of three independent tracking layers (L1-L3), each providing a 3-D reconstruction of space points along the track with a 2-D readout.

Each layer will be a cylindrical GEM detector. The CGEM is a triple-GEM detector composed by concentric cylindrical electrodes (Fig. 2.1): the cathode (the innermost electrode), three GEM foils, and the readout anode (the outermost electrode). The spacing between the cathode and the first GEM foil (the conversion gap) is 3 mm, while all the other gaps are 2 mm.

The readout anode of each CGEM is segmented with 650  $\mu\text{m}$  pitch XV patterned strips with a stereo angle that changes depending on the layer geometry. The full system consists of about 10,000 electronics channels.

This technology allows the construction of a light and fully sensitive detector, that can match the stringent requirement on the material budget needed to minimize the multiple scattering effect for low-momentum tracks and improving the current vertex resolution of the apparatus. Moreover, the good timing resolution and the high rate capability of the GEM (up to 1 MHz/mm<sup>2</sup> [?]) makes such detectors suitable to be placed near the interaction point of a high-luminosity collider machine.

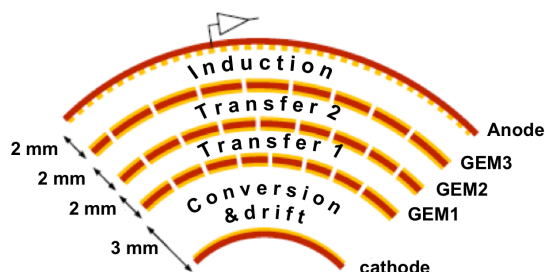


**Figure 2.1:** Schematic of triple cylindrical GEM detector.

### 2.1 Operating Principle of a Triple Cylindrical GEM Detector

A GEM (Gas Electron Multiplier) detector is made by a thin (50  $\mu\text{m}$ ) Kapton foil, copper clad on each side, with a high surface density of holes [?]. In the standard technique each hole has a bi-conical structure with external (internal) diameter of 70  $\mu\text{m}$  (50  $\mu\text{m}$ ); the hole pitch is 140  $\mu\text{m}$ . The bi-conical shape of the hole is a consequence of the double mask process used in standard photolithographic technologies. The GEM foils are manufactured by the CERN EST-DEM workshop <sup>1</sup>.

A typical voltage difference of 300 to 500 V is applied between the two copper sides, giving fields as high as 100 kV/cm into the holes. Those fields multiply the numbers of the electron produced by a charged particle crossing the detector by a factor up to a few thousand. Multiple structures realized by assembling two or more GEMs at close distance allow high gains to be reached while minimizing the discharge probability [?].

#### 2.1.1 The KLOE-2 Inner Tracker: Know-How and status

The KLOE-2 Collaboration built the only existing CGEM based detector [?, ?], currently under commissioning [?]. Due to the operational delays of DAΦNE, the accelerator on which the KLOE-2 is set, no real data taking could be performed in order to investigate the performances and the data stream of the KLOE-2 CGEM-IT.

Once the first results will be published or presented by the KLOE-2 Collaboration, this section will be updated.

### 2.2 BESIII CGEM Innovations

**COMMENT: Author(s): Savrie', Baldini, Marcello, Felici**

1. CERN EST-DEM is the Design and Manufacture of Electronic Modules (DEM) Group of the Engineering Support and Technology Division (EST) [http://ts-dep-dem/](http://ts-dep-dem.web.cern.ch/ts-dep-dem/)

The design and the construction of the KLOE-2 CGEM detector allow the present project not to start from scratch. Several of the people involved in the present proposal did participate to the KLOE-2 CGEM detector development and commissioning, acquiring a valuable expertise that allow us to replicate what worked best in the KLOE-2 experience and to further proceed by introducing new innovative concept in the design and construction of the BESIII CGEM-IT detector. The innovative aspects are mainly related, but not limited, to the following three items: the material used to give the mechanical rigidity to the detector structure (that will be Rohacell instead of Honeycomb), the anode design, and the different readout mode. In this subsection we'll briefly summarize such innovations while a detailed discussion of the overall detector design and construction will be addressed in Sec. 3.

### 2.2.1 Rohacell

A new Rohacell based technique will be adopted to manufacture the anode and cathode structures in order to minimize the material budget with respect to the current state of the art of the detectors.

The Rohacell [?] is the trade name of a PMI-based structural foam that is used in fiber-composite technology and which main characteristics are excellent mechanical properties over a wide temperature range, even at low densities, high temperature resistance up to 220°C, unique compressive creep behavior for processing up to 180°C and 0.7 MPa, excellent dynamic strength and cell sizes that can be tailored for each processing method. Rohacell's homogenous cell structure provides zero print through to the composite face sheets leaving a class A surface finish every time.

Rohacell is available in different densities; we will use 31 IF/IG-F type, which is the lightest one, having a density of 32 kg/m<sup>3</sup> and available in foils of different dimensions and thickness. We found out that a thickness of 2 mm is suitable for our application.

Building supports for the sub-layers composed of Rohacell instead of the standard Honeycomb allows to significantly reduce the total radiation length of detector compared to equivalent structure composed by Honeycomb while maintaining the mechanical robustness. In addition, the Rohacell is more homogenous with respect to the Honeycomb, and that is also an advantage for the tracking system.

### 2.2.2 Anode design

The anode design is one of the main element of difference with respect to the KLOE-2 CGEM. It has been developed on the basis of the readout used by the Compass experiment [?] with some potential improvements studied with simulations that will be confirmed with tests on prototypes (see Sec. 2.2.4) before the final construction.

The readout anode circuit is also manufactured by EST-DEM CERN Workshop starting from the 5  $\mu\text{m}$  copper clad, 50  $\mu\text{m}$  thick polyimide substrate, the same used for GEM foils. Two such a foils with copper segmented in strips will be used to have the two dimensional readout. The strip pitch will be 650  $\mu\text{m}$ , 570  $\mu\text{m}$  wide X-strips are parallel to CGEM axis, providing the  $r\varphi$  coordinates; while the V-strips, having a stereo angle with respect to the X-strips, are 130  $\mu\text{m}$  wide and, together with the other view, gives the  $z$  coordinate. The stereo angle depends on the layer geometry and will be 45.9 deg for layer 1, -31.1 deg for layer 2 and 33.0 deg for layer 3.

A jagged-strip layout (shown in Fig. 2.2) has been studied to minimize the strip capacitance: the inter-strip capacitance reduction compared to the standard linear strip configuration (also shown in Fig. 2.2) is about 30% as shown in Fig. 2.3.

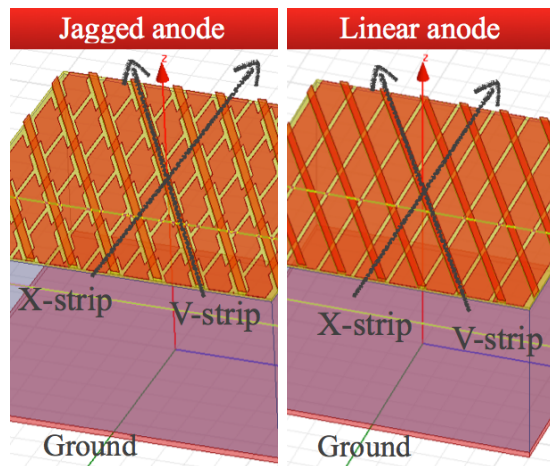


**Figure 2.2:** Left: the *jagged* layout where the overlap between the strips is reduced by decreasing the size of the X-strips on the intersections in order to minimize the inter-strip capacitance. Right: standard linear strip configuration.

Another significant difference with respect to the anode design made by KLOE-2 experiment is the ground plane that is brought to a distance of 2 to 4 mm in order to reduce the capacitance coupling between strip planes and the reference voltage. The

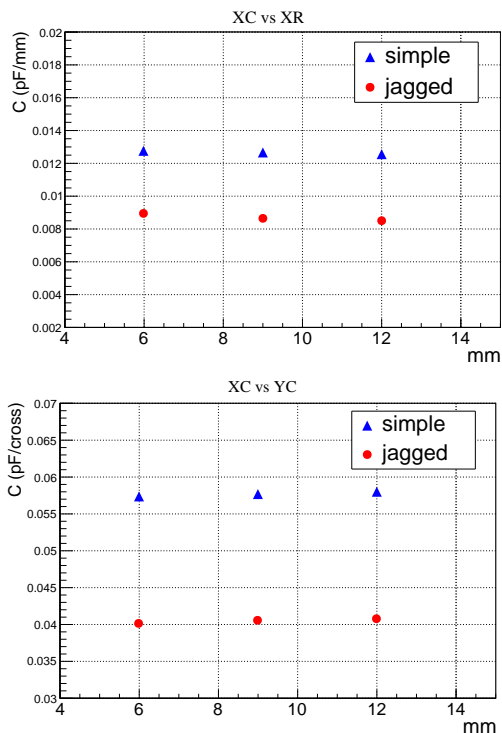


**Figure 2.3:** Comparison of the capacitance between two single adjacent strips (top) and of X vs V strip (bottom) for prototype of different dimensions.

space between the readout plane and the ground will be filled by a Rohacell structure. The comparative analysis of the capacitance couplings of the two configurations is performed by means of Maxwell simulations [?].

Additional studies on the anode configuration will be performed with Garfield simulations software [?] in order to extract useful information for the charge sharing and the hit digitization, which are relevant for the analog readout and the full simulation of the detector. Studies with a small  $10 \times 10 \text{ cm}^2$  planar prototype equipped with the BESIII baseline anode configuration will provide valuable input for the simulations and a final validation of the readout design (see Sec. 2.2.4).

### 2.2.3 Analog vs Digital Readout

To achieve the required spatial resolution of the order of  $100 \mu\text{m}$  both binary and analog strip readout method have been investigated. The first one identifies clusters by detecting adjacent strips with a collected charge above a fixed threshold; the reconstructed position of the track is the geometrical center of the cluster and the resolution is (roughly) defined by the ratio  $pitch/\sqrt{12}$ .

The analog readout method, on the other hand, allows to set both a threshold on the single strips and a threshold on the total charge then improving the ghost hit rejection (a ghost hit is an over threshold cluster due to noise). Moreover, the strip collected charge encoding allows the reconstruction of the charge centroid, then boosting the resolution above the  $pitch/\sqrt{12}$  ratio of the binary readout method.

Concerning the hardware requirements, the binary readout front-end can be easily implemented as it manages only a single bit information per strip, while the analog readout front-end requires the encoding of the collected charge and, as a consequence, a more complex readout chain (each channel must include a digitization section).

The easier implementation of the binary readout chain anyway has a not negligible drawback. Due to the constraint in spatial resolution requirement (of the order of  $100 \mu\text{m}$ ) the strip pitch should be  $\simeq 300 \mu\text{m}$ , and, consequently, the number of channels to fully readout the detector would amount to about 25 thousand then causing troubles in terms of power consumption, number of cables and space required to host the on-detector electronics.

The analog readout chain, on the other hand, allows a larger strip pitch ( $500\text{-}650 \mu\text{m}$ ) then resulting in a more manageable number of channels (about ten thousand).

Because of the strong constraints in terms of space, power consumption and spatial resolution, as well as noisy hit rejection capability, the analog readout method has been chosen to implement the CGEM IT readout chain, which will be described in Chapter 4.

### 2.2.4 Planar Test Setup

The design of the BESIII CGEM-IT readout anode is different from the KLOE-2 one, and also the grounding scheme. A planar test setup allows inexpensive and relatively fast test of a portion of a complete detector layer. The setup is based on the following components:

- Trigger
- Tracking system
- DAQ
- The test chamber

The complete setup, assembled in Frascati, is shown in Fig. 2.4.

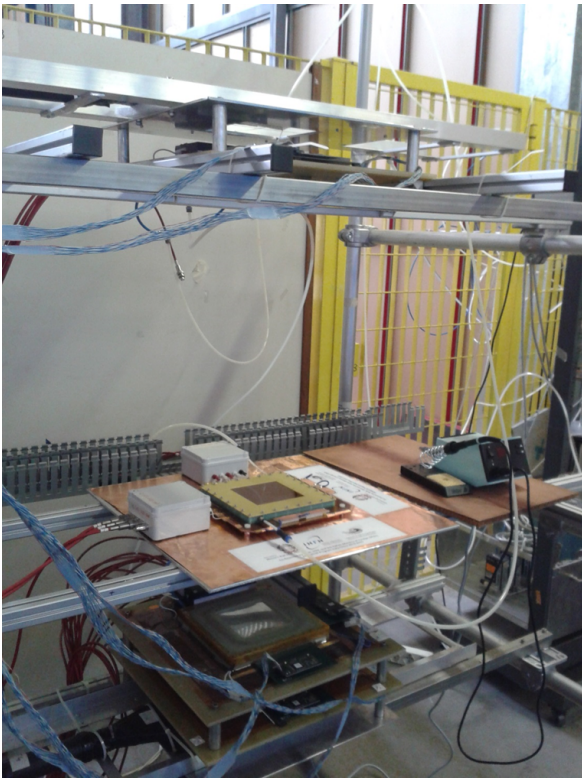


**Figure 2.4:** The planar test setup in Frascati.

### The trigger

The cosmic trigger is composed by two plastic scintillators, of approximate dimensions  $10 \times 10 \text{ cm}^2$ , separated vertically by a distance of 1 m, read out by two Hamamatsu PM. The PM output is fed to common NIM electronics for discrimination and coincidence. The coincidence, with an approximate rate of 0.1 Hz, triggers the DAQ electronics in a VME crate (see below) and a Tektronix TDS640A for monitoring and auxiliary measurements.

### The Tracking System

The KLOE-2 group has contributed three small tracking chambers having the same GEM structure as the main cylindrical KLOE-2-IT: a drift region 3 mm wide, followed by three transition gaps 2 mm wide. Each chamber has separate X and Y readouts of 120 strips with pitch equal to  $650 \mu\text{m}$ , so that the active area is of about  $8.3 \times 8.3 \text{ cm}^2$ .

The gas mixture used is Ar/Isobutane 90%/10%; we make the mixture using 2 MKS mass flowmeters and a 647C digital controller. The 2 flowmeters are accurate to 0.1% of the full ranges, respectively 500 and 50  $\text{cm}^3/\text{min}$ , so the flows are  $(90 \pm 0.5) \text{ cm}^3/\text{min}$  and  $(10 \pm 0.005) \text{ cm}^3/\text{min}$ . The flows are

monitored approximately once every 3 seconds via the 647C serial port and a MOXA 5450 device, that makes available the 647 serial interface on an Ethernet port. The gas monitor, in LabView, interlocks the HV system: in case of irregularities in the flow of Isobutane, all tracking chambers are shut off to avoid damage to the GEM regions. A hardware interlock, based on a pressure sensor inline with the isobutane flow and an Arduino processor is also being developed and should be available soon.

The HV System is based on a CAEN SY1527LC chassis with 2 A1550 boards, for a total of 36 HV channels: each tracking chambers requires 7 separate HVs. The software, contributed by the KLOE-2 experts, ramps coordinately all 7 channels of one chamber, so that temporary overvoltages on different sides of a GEM foils are not possible. The currents drawn by the KLOE-2 tracking chambers and the BESIII test one are read out via a nanoAmperometer designed and made by the LNF SELF electronics service and is the final one that we expect to use on the BESIII CGEM-IT.

### The DAQ system

Each tracking chamber is read out via 2 GASTONE64 [?] digital chips for each view: the 12 GASTONE chips are run by 3 controllers in VME boards, readout is initiated automatically by the cosmic trigger discussed above. The DAQ PC read out the VME crate via an USB connection, perfectly adequate for a slow cosmic trigger, and a CAEN V1718 controller.

### The test chamber

This chamber is currently being ordered at CERN and will carry the final BESIII readout layer type. Another one has been available for a while, with a readout more similar to the COMPASS one, and has been useful to debug the system, via the currents drawn.

We expect to be able to read both test chambers soon (and compare performances) with an APV25 system [?].

### Preliminary results

We have been able to obtain a measurement of resolution of the tracking chambers.

In Fig. 2.5 we show the distance between hits in the middle KLOE-2 tracking chamber and the extrapolation of the line measured by the top and bottom

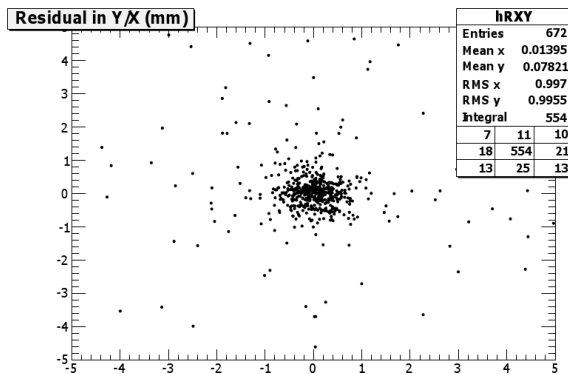


**Figure 2.5:** Tracking resolution of the LNF cosmic setup.

ones, in both the X and Y view. The fitted resolution of the central peak, on a very small background of casual hits, is of about  $400 \mu\text{m}$  micron, but includes systematics due to possible small chamber misalignment. In the present setup chambers are not securely fastened to a common structure, we are designing a special fixture to keep under better control the positioning, that will also allow secure rotation of the system by 90 degrees, for possible use in particle beams test.

## References

- [1] M. Alfonsi et al. *Nucl. Instrum. Methods A*, 50258, 2009.
- [2] F. Sauli. *Nucl. Instrum. Methods A*, 386:531, 1997.
- [3] S Bachmann et.al. *Nucl. Instrum. Methods A*, 479:294, 2002.
- [4] A. Balla, G. Bencivenni, S. Cerioni, P. Ciambrone, E. De Lucia, et al. Status of the Cylindrical-GEM project for the KLOE-2 inner tracker. 2009.
- [5] A. Balla, G. Bencivenni, M. Capodiferro, S. Cerioni, P. Ciambrone, et al. A new cylindrical-GEM inner tracker for the upgrade of the KLOE experiment. *Nucl.Phys.Proc.Suppl.*, 215:76–78, 2011.
- [6] A. Balla, G. Bencivenni, P. Branchini, A. Budano, M. Capodiferro, et al. Production and test of the first two layers of the KLOE-2 Inner Tracker. *Nucl.Instrum.Meth.*, A718:416–417, 2013.
- [7] <http://www.rohacell.com/product/rohacell/en/about/properties/pages/default.aspx>.
- [8] et al P. Abbon. *arXiv:hep-ex/0703049*, 2007.
- [9] <http://www.ansys.com/Products/Simulation+Technology/Systems+&+Multiphysics/Multiphysics+Enabled+Products/ANSYS+Maxwell>.
- [10] <http://garfield.web.cern.ch/garfield/>.
- [11] A. Balla, G. Bencivenni, P. Branchini, A. Budano, S. Cerioni, et al. GASTONE64: A new front-end ASIC for the cylindrical GEM Inner Tracker of KLOE-2 experiment at *DAΦFNE*. *Nucl.Instrum.Meth.*, A732:523–525, 2013.
- [12] B. Ketzer, S. Bachmann, M. Capeans, M. Deutel, J. Friedrich, et al. GEM detectors for COMPASS. *IEEE Trans.Nucl.Sci.*, 48:1065–1069, 2001.



## 3 The BESIII CGEM-IT

---

**COMMENT: Author(s): Cibinetto, Calcaterra**

In this section we will first review the CGEM-IT expected performances with respect to the existing Drift Chamber IT, then we will discuss the overall mechanical design of the new IT and finally the construction procedure will be presented together with the tooling needed for the assembly.

### 3.1 CGEM-IT vs DC-IT

**COMMENT: Author(s): Baldini, Maggiora**

GEM detectors are characterised by high radiation hardness, high rate capability and allow for a flexible geometry. The layout proposed for the BESIII CGEM-IT and described in the following sections introduces a reduced material budget (about 1% of radiation length). Thanks to the analog readout described in Sec. 2.2.3, CGEM-IT is expected to provide very good spatial resolution:  $\sim 100 \mu\text{m}$  in the  $r\phi$  view and  $\sim 200 \mu\text{m}$  in the  $rz$  view, to be compared with the  $\sim 120 \mu\text{m}$  in the  $r\phi$  view and  $\sim 0.2 \text{ cm}$  in the  $rz$  view provided by the current DC-IT.

In both these IT's the determination of the  $z$  coordinate is achieved by means of stereo angles in the different layers: between the wires in the IT and between the strips in the CGEM. But while in the DC-IT the stereo angles are limited to few degrees, essentially by the distortion of the electric field into the drift cell, in the CGEM-IT the only limitation comes from the number of foils that can be included in the anode plane. The layout proposed for the CGEM-IT in the following sections of this chapter foresees a single foil in the most inner layer, leading hence for such a layer to a  $45.9^\circ$  stereo angle, and two foils in the outer layers, that are hence characterised by  $-33.1^\circ$  and  $33.0^\circ$  stereo angles. By choosing a negative stereo angle for the middle layer it is possible to double the difference in the stereo angles between the central and the inner and outer layers of the CGEM-IT.

The larger stereo angles of the CGEM-IT allow hence for a quite better  $rz$  resolution w.r.t. the DC-IT, but at the same time cause as a drawback the increase of ambiguities in associating the  $r\phi$  and the  $rz$  views. In fact, if the stereo angle is

very small, as in the DC-IT case, the wrong associations are unphysical, being mostly outside the chamber. However, in the present CGEM proposal, since the stereo angles between the CGEM layers are quite different, the wrong associations are not at all aligned and they can be ruled out already at the CGEM pattern recognition level. The number of wrong associations still aligned depends on the resolutions and on the number of tracks impinging on the same CGEM foil, but preliminary studies let us expect that it should be limited, at a few per mille level in the worst case of 6 charged tracks on a single CGEM foil and of a few millimeters resolutions at the pattern recognition level. The background at small angles might be a concern, and although it had not yet been implemented in the preliminary studies leading to the figure depicted here and in Sec. 7.3, it will be investigated in details as soon as the software framework specifically developed for the CGEM-IT and described in Chap. 7 will be in a more mature stage.

A preliminary estimation of the expected background rates in the CGEM-IT has been obtained making use of the framework described in Sec. 7.1, and in particular of the CGEM-IT geometry, and reported in Sec. 1.2. While the physically meaningful quantity in the case of the DC-IT is the background rate per wire, when considering the CGEM-IT the key quantity is the background rate per strip: the expected rates, assuming the strip pitch described in Sec. 3.2.2, are compatible with the current design of the on-detector electronics (see Sec. 4.3).

Our preliminary studies let us expect for the CGEM-IT resolutions comparable with the DC-IT both in the  $rz$  view ( $\sim 5\%$  poorer for low momentum tracks) and in momentum ( $\sim 5\%$  better for large momentum tracks), while the resolution in the  $rz$  view is expected to be significantly improved and at least doubled.

Such improved detector performances w.r.t. the current DC-IT could be exploited in order to further optimise the reconstruction in BESIII of secondary vertices and in particular to increase the detection efficiency of those secondary vertices corresponding to the decays of particles with particularly low  $c\tau$ . A first preliminary estimation with a toy Monte Carlo simulation is reported in Sec. 7.3; this issue as well will be investigated in details once a full tracking for the CGEM-IT will be included in the offline software.

## 3.2 Mechanical Design

**COMMENT: Author(s): Cibinetto, Calcaterra**

The space available in the inner part of the BESIII spectrometer is quite limited, and this introduces significant constraints on the mechanical design and on the power dissipation per readout channel. The mechanical design of the detector must take into account several constraints: the mechanics of the interaction region (i.e. beam pipe, existing flanges, magnets, and the outer Drift Chamber), the fact that the frontend boards need to be placed “on” the detector in order to minimize the noise pickup and to avoid signal degradation; the placement of the high voltage distribution cards at the edges of detector. Therefore the mechanical design needs to be very compact and optimized.

The radial dimension of the CGEM-IT is limited internally by the beam pipe and externally by the Drift Chamber carbon fiber cylinder that will be installed once the inner chamber will be removed in order to seal the outer one. This sticks the CGEM-IT inner radius at 78 mm and outer radius at 179 mm.

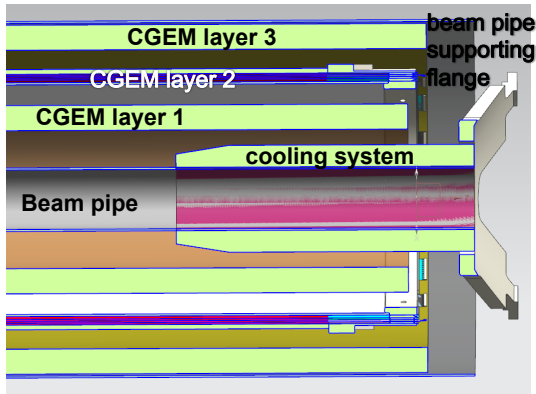


**Figure 3.1:** Cross section of a portion of the interaction region of BES-III instrumented with CGEM-IT.

More tricky is the situation along the  $z$  direction where the space available for the detector, the frontend electronics and utilities is limited by the set of flanges that holds the beam pipe and that will be used also to support the CGEM-IT. A lateral section of the interaction region is reported in Fig. 3.1; the space available at the edges of the detector is about 80 mm for each side.

A compact mechanical interface, called “service flange” is to be designed in order to host the high voltage distribution boards, the gas lines, the cooling system and to smooth the signal and power ca-

ble routing. The service flange will be made of Permaglass (G11) in order to prevent accidental high voltage discharge, and it will be used as interface between the detector and the beam pipe supporting flange, holding each layer independently.

In order to free as much space as possible the mechanical length of the three layers will be slightly incremental with the radius as shown in Fig. 3.1. In addition, at least in the first and in the second layer, the frontend electronics cards will be located in the dead space available between the layers outside the active area, as shown in Fig. 3.2.

Proper tooling will be needed to install the CGEM-IT. Additional details on the integration of the CGEM-IT with the BESIII detector are discussed in section 6.1.

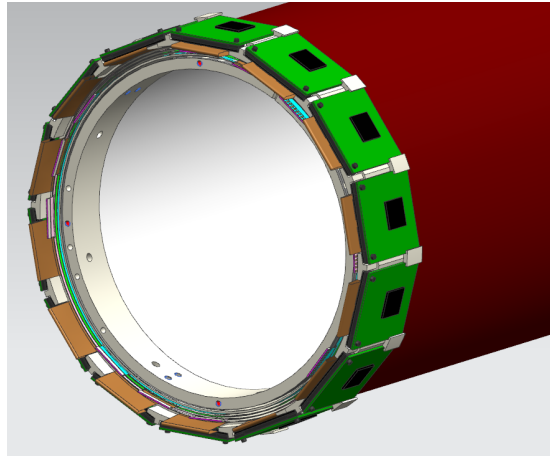


**Figure 3.2:** Drawing of the layer 2 CGEM showing the frontend cards located on the anode Permaglass ring.

### 3.2.1 Construction Technique

A special assembling technique has been developed by KLOE-2 to obtain cylindrical GEM electrodes [?]. Two GEM foils are glued together on a plane to obtain the single large foil needed to make a cylindrical electrode. Epoxy is applied on one of the sides of the GEM foil, on a 3 mm wide Kapton region<sup>1</sup>. Then the foil is rolled on an aluminum mold coated with a very precisely machined 400  $\mu\text{m}$  thick Teflon film which provides a non-sticky, low friction surface. For each GEM foil a different mold is used. Finally the mold is inserted in a vacuum bag, and vacuum is made providing a uniform pressure over the whole surface of the cylinder. Two Permaglass annular rings are glued on the edges of the electrode, acting as spacers for the gaps and providing

<sup>1</sup> This procedure will not be needed for layer 1, which is the smallest, and can be assembled with just one foil.

all of the mechanical frames needed to support the detector as shown in Fig. 3.3. After the curing cycle of the glue, the cylindrical electrode can be easily extracted from the mold thanks to the Teflon surface. Cathode and anode are obtained with a similar procedure.

The assembly of the five electrodes proceeds from the outermost electrode (the anode) to the innermost one (the cathode). Fig. 3.4 displays a lateral section of an assembled layer showing the Permaglass rings acting as spacers between the layers.

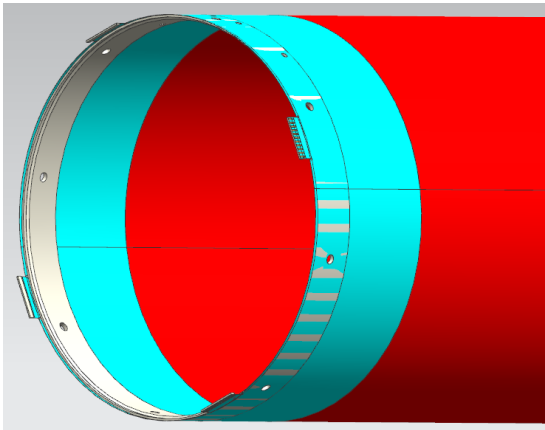


**Figure 3.3:** 3D model of a cylindrical GEM foil with the Permaglass rings at the edges.

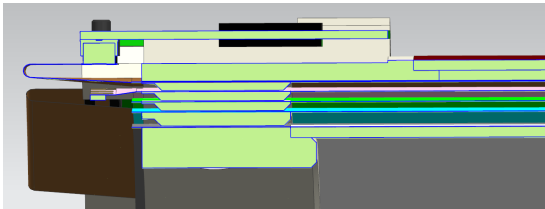


**Figure 3.4:** Lateral section of the Layer 2 showing the Permaglass rings acting as spacers between the electrodes.

### 3.2.2 Detector Components

**The cylindrical cathode.** The cathode foils are produced by the CERN EST-DEM workshop as polyimide foils,  $50\ \mu\text{m}$  thick, with a copper cladding of  $3\ \mu\text{m}$  on the internal surface. One foil will be used for Layer 1, and two foils for each of the other layers. The cathode cylindrical structure will be composed by two 1-mm Rohacell layers. Rohacell foils, cut in helicoidal shape, will be rolled around the molds; two helicoids, left and right handed, will be needed in order to assure the best robustness of the structure. For a better gluing, a  $12.5\ \mu\text{m}$  thin, Kapton

foil will be placed between Rohacell the two layers. The Rohacell is machined very precisely to 1 mm of thickness by means of a lathe. This technique has been successfully tested, In Ferrara, on cathode and anode prototypes of different dimensions as shown in Fig. 3.5.



**Figure 3.5:** Top: machining of the Rohacell during the fake cathode construction. Bottom: a picture of the fake cathode with the radius of the innermost layer of the CGEM-IT.

The cathode will be glued on top of this structure. The mechanical support of the chamber is composed by annular flanges made of Permaglass placed on the edges of the cylinder. These rings house the gas inlets and outlets and their thickness defines the space of the gap between the cathode and the first GEM.

**The GEM foils.** In Layer 2 and 3, two GEM foils are spliced together in order to realize one single electrode. For a safe detector operation each foil has independent high voltage sectors, in order to limit the capacitance and hence the energy released through the GEM hole in case of discharges. Each foil is divided in sectors, 40 for layer 1 and 2, and 60 for layer 3. The capacitance of each sector of the different layer is reported in table 6.1.

**The anode readout.** The anode will be manufactured by the CERN EST-DEM as two layers of 50  $\mu\text{m}$  thick Kapton foils with 3.5  $\mu\text{m}$  copper strips, providing a 2-D readout. The strip pitch is 650  $\mu\text{m}$  and will be the same for both the views. The X-strips will be 570  $\mu\text{m}$  wide and provide the azimuthal coordinate. The other coordinate is given by the V-strips, that are 130  $\mu\text{m}$  wide and intersect the X-strips with a stereo angle that depends on the layer geometry. The strip dimensions are chosen in order to equally share the charge on the strips of the two view, while their pitch allows the achievement of the desired spatial resolution keeping the number of channels manageable. The anode plane will be rolled on its proper mold and then, two 2-mm Rohacell layers will be glued on top of it, with a 12.5  $\mu\text{m}$  Kapton foil between them. At the end the ground plane will be glued. As for the cathode and for the GEM, also for the anode a special set of Permaglass annular rings will be placed on the edges of the cylinder.

### 3.2.3 Material Budget

The combination of Rohacell support structure and the new anode configuration makes the CGEM-IT an incredibly light detector, only about 1% of radiation length ( $X_0$ ) in total. The breakdown of material budget calculation is reported in tables 3.1, 3.2 and 3.3. An additional 0.042 % of  $X_0$  have to be added to consider a Faraday cage around the detector. Finally the carbon fiber cylinder, needed to seal the outer drift chamber, has to be included.

**Table 3.1:** Material budget calculation for the CGEM-IT cathodes.

material	thickness ( $\mu\text{m}$ )	fill factor	Radiation length (%)
kapton	12.5	1	0.004375
rohacel	1000	1	0.007
kapton	12.5	1	0.004375
rohacel	1000	1	0.007
kapton	12.5	1	0.004375
kapton	50	1	0.0175
copper	3	1	0.021
Total			0.065625

## 3.3 Tooling and Construction

**COMMENT: Author(s): Cibinetto, Calcaterra**

**Table 3.2:** Material budget calculation for the CGEM.

copper	3	0.8	0.0168
kapton	50	0.8	0.014
copper	3	0.8	0.0168
Total			0.0476

**Table 3.3:** Material budget calculation for the CGEM-IT anodes.

copper	3	1	0.021
kapton	50	1	0.0175
rohacel	2000	1	0.014
kapton	12.5	1	0.004375
rohacel	2000	1	0.014
kapton	50	1	0.0175
copper	3.5	0.87	0.021315
kapton	50	0.2	0.0035
copper	3.5	0.2	0.0049
Total			0.11809

### 3.3.1 Quality Controls and preliminary operations

Before the final assembly of the different parts of the detector, each component follows a well defined preparation procedure that includes a global optical inspection, a cleaning and an HV test. In particular for GEMs the HV test is repeated at each construction step, in order to avoid the assembly of damaged GEM and to minimize the losses of precious components, and of the time needed to reorder them.

#### 3.3.1.1 Visual inspection and electrostatic tests

GEMs do not require any special cleaning procedure, because in principle they are clean: the only allowed cleaning procedure is done with a light nitrogen flush that is generally used to gently remove possible dusts. Any other procedure can damage the GEM. A first optical inspection is done by eye: we look for areas with possible defects, typically spots with unavoidable inhomogeneity in the material as local absence of the metal and underlying Kapton or lack of holes. A more careful optical inspection of these spots is then performed under microscope, equipped with a digital camera in order to evaluate the dimension and type of the defect. Such defects have generally little consequence in the operating behavior of the GEM, unless they are too big or too frequent. Acceptance criteria for GEMs to be used in the CGEM-IT are: not more than one

defect with an area less than  $1 \text{ mm}^2$  per each GEM sector.

The HV test of a GEM is performed inside a gas tight box flushed with Nitrogen, in order to reduce the ambient humidity down to 10% (time needed about 5 hours). The HV is applied individually to each sector through a  $500 \text{ M}\Omega$  limiting resistor, in order to avoid GEM damage in case of discharges, while the non-sectored side is grounded. The maximum current rent in the power supply is set to 100 nA. The HV is slowly increased with eighteen steps up to a maximum of 600 V:

- from 0 to 400 V with 50 V steps of 20 seconds each;
- from 400 V to 500 V with 25 V steps of 60 seconds each;
- from 500 V to 600 V with 10 V steps of 2 minutes each.

The GEM sector pass the HV step if the current is less than 1 nA and no more than 3 discharges occurred during the test time. In case these acceptance requirements are not fulfilled the voltage ramp-up on the sector is suspended and the test is repeated later on.

### 3.3.2 Obtaining cylindrical GEM and electrode foils

The KLOE-2 group [?] devised an accurate procedure to obtain cylindrical flexes starting from planar GEM foils, manufactured at CERN. We are much indebted to them, both for showing and explaining to us the procedure, and for the bulk of this description as well.

#### 3.3.2.1 GEM foils

We start by positioning two GEM foils, previously subjected to Quality Controls and –if necessary– trimmed to the right dimension, side by side on a glueing table, as shown in Fig. 3.6.

We apply an Araldite-based epoxy to one of the short sides of the GEM foil, on a 3 mm wide region. Then the foil is rolled on an aluminum mould coated with a very precisely machined  $400 \mu\text{m}$  thick Teflon film which provides a non-stick, low friction surface, and another glueing stage occurs along the side of the cylinder. The mould is inserted in a plastic bag in which vacuum is made with a Venturi system,

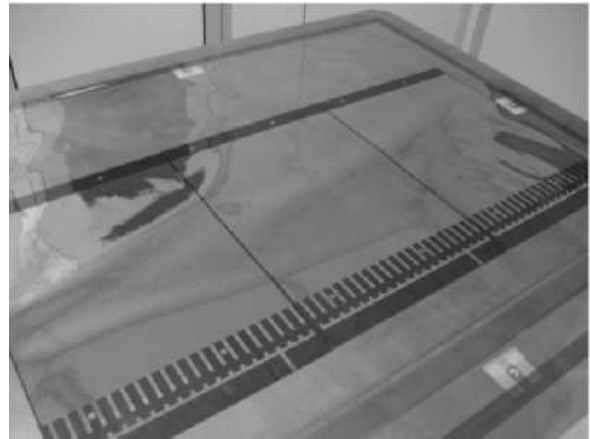


**Figure 3.6:** One of the KLOE-2 complete GEM layers. BESIII GEM layers will be composed of only 2 GEM sheets, because of the BESIII CGEM-IT smaller radius.

resulting in a uniform pressure of  $0.8 \text{ kg/cm}^2$  over the whole surface of the cylinder.

This pressure is maintained for the glue curing time of 12 hours. At this stage, two fiberglass annular rings are glued on the edges of the electrode, acting as spacers for the gaps and providing the mechanical frames needed to maintain the cylindrical shape detector. After another glueing stage, the cylindrical electrode can be covered for cleanliness, and remain stored on its mold until all 5 cylindrical components of one detection layer have been manufactured.

At assembly time, all 5 layers will be safely and easily separated from their moulds by sliding them in the axial direction, thanks to the low-friction Teflon surfaces.

#### 3.3.2.2 Cathode construction

The cathode is similar to the KLOE-2 cathodes, the main differences are that its thickness and radiation lengths are reduced since the reinforcing structure is realized with Rohacell, a material having better mechanical properties and longer radiation length than the epoxy/cardboard honeycomb used in KLOE-2. The cathode is realized as a splicing of two foils for the outermost two CGEM-IT layers, but one foil is enough for the innermost layer.

#### 3.3.2.3 Anode construction

Also the anode is realized as a splicing of two foils for every layer, except for layer one, each with the readout copper strips. Similarly to the cathode, the reinforcing structure will be made of Rohacell. The ground plane will be glued on to of the Roha-



**Figure 3.7:** Two electrodes fixed on the vertical insertion system used to assembly the KLOE-2 detector.

cell structure. But the electrical structure will be much different, deriving with modifications from a COMPASS-type design. It has been described in detail at the end of Sec. 3.2.

#### 3.3.2.4 Assembly of the detector

The five electrodes are extracted from the moulds along the vertical direction by using a PVC ring, fixed with pins to one of the annular flanges of the cylinder, and then are inserted one into the other. To accomplish the insertion of the electrodes without damaging the GEMs, a dedicated tool has been realized: the Vertical Insertion System (see Fig. 3.7).

The system is designed to permit a very precise alignment of the cylindrical electrodes along their vertical axis. The bottom electrode is fixed, while the top one is slowly moved downwards by a manually controlled step-motor, coupled with a reduction gear system. The operation is performed with the help of three small web-cameras, placed at 120 degrees one to each other around the top cylindrical electrode, thus allowing the monitoring of the radial distance between the electrodes (2-3 mm typically). The up-down rotation of the assembly tool allows

an easy sealing of the detector on both sides.

## References

- [1] et al. F. Archilli. Technical report.

## 4 Front End Electronics

**COMMENT: Author(s): Marcello, Felici, Johansson, Marciniewski**

### 4.1 Requirements

The CGEM-IT has been designed to replace the BESIII inner drift chamber in order to avoid deterioration of its performance due to radiation background.

The three CGEM layers aim to archive an overall spatial resolution better than  $100 \mu\text{m}$  for tracking purpose, a time resolution of the order of  $5 \text{ ns}$  (assuming low occupancy) for correct event reconstruction, a good transparency to the radiation and, finally, minimize inefficiencies due to pile-up effects. The spatial resolution goal has been already discussed in Sec. 2.2.3, the two other goals are shortly discussed in the following.

#### 4.1.1 Time resolution

BEPCII collider operates with 93 bunches spaced  $8 \text{ ns}$ , while the MDC time measurements rely on the HPTDC (High Performance TDC) chip developed at CERN and a delivered system clock of  $24 \text{ ns}$ , corresponding to 3 bunches duration. When a good event is generated by a collision the time measured by the HPTDC correspond to the difference between the start time (i.e. the  $24 \text{ ns}$  clock leading edge) and the arrival time of the signal in the detector. As a consequence, because of the difference of the main system clock and the bunch crossing period ( $24 \text{ ns}$  and  $8 \text{ ns}$ ), it is not possible to determine the collision time by means of the online system and calculation must be carried out by means of the offline data analysis. Then, assuming low occupancy,  $4\text{-}5 \text{ ns}$  overall time resolution should allow correct track reconstruction.

#### 4.1.2 Dead Time Estimation

The system dead time (i.e. the time after each event during which the system is not ready to record a new event) determines the probability that two or more events overlap (pile-up), therefore it should be as short as possible.

The dead time has two contributions: the intrinsic detector dead time (i.e. the drift time for gaseous

detectors) and the readout contribution (for example the shaping time of front-end amplifier or the analog to digital conversion time). As it will be explained in Sec. 4.3 the total drift time of a GEM detector is below  $200 \text{ ns}$ , then the readout contribution must be modulated according to a certain value of the pile-up probability. As an example, the dead time as a function of the average input rate for different pile-up probabilities is shown in Fig. 4.1, according to the Poisson distribution of Eq. 4.1:

$$P(N, \Delta T) = \frac{(\bar{n}\Delta T)^N}{N!} e^{-\bar{n}\Delta T} \quad (4.1)$$

For instance, setting a pile-up probability of  $3 \%$  and taking into account the single channel rate of  $60 \text{ kHz}$ , the overall system dead time should be less than  $0.6 \mu\text{s}$ .

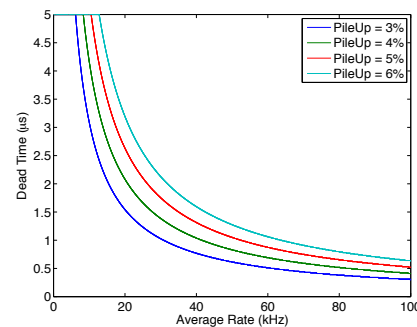


**Figure 4.1:** Dead time vs rate for different pile-up probabilities

### 4.2 System Block Description

The readout chain can be divided into two blocks as shown in fig. 4.2

- **ON DETECTOR** electronics: Preamplifier Boards located on the detector to preserve the strips S/N ratio.
- **OFF DETECTOR** electronics: Readout Boards and Concentrator Boards located as close as possible to the detector.

The requirements for both blocks will be briefly discussed in the following paragraphs.

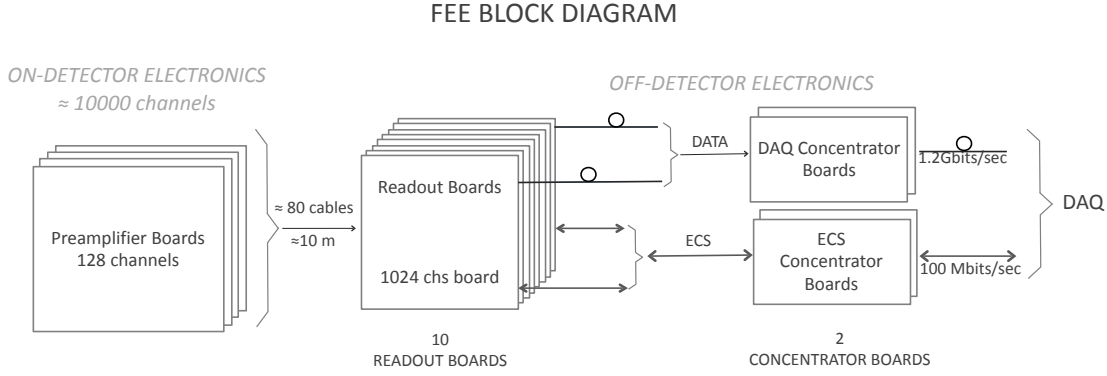


Figure 4.2: CGEM IT front-end electronic chain block diagram

## 4.3 On-Detector Electronics

### 4.3.1 Charge Measurement Specifications

Because we aim to implement a charge centroid measurement, the encoding (ADC) requirement in terms of number of bits is moderate. According to the measurements carried out at CERN (Fig. 4.3) without magnetic field, the charge distribution, for a minimum ionizing particle (mip) impinging orthogonally the detector, is about 1.5 mm wide. Further measurements carried out by the LNF-INFN group [?] have highlighted a spread in the charge distribution due to the gas gain and the magnetic field, as shown in Fig. 4.4.

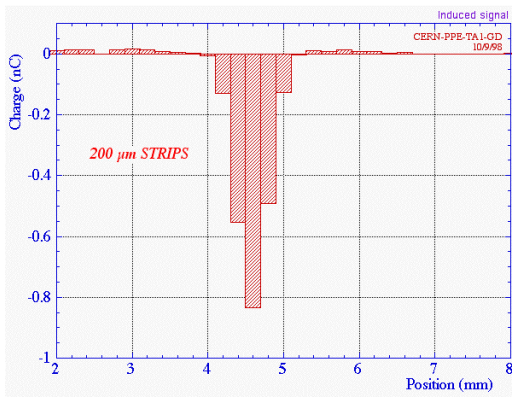


Figure 4.3: Cluster Charge Distribution (200 μm pitch strips) without magnetic field

In the worst case (high gas gain and high magnetic fields), assuming a 650 μm pitch about 3 strips are interested by a single ionizing event (note: the num-

bers shown in Fig. 4.4 must be considered as a lower limit, because binary readout method has been used in the measurement).

An evaluation of the position resolution of a localized avalanche has been carried out in 1990 by Debbe, Radeka and O'Brien [?]. They found that the achievable resolution could be expressed by the following relation (4.2)

$$\sigma_s = \frac{\sqrt{n-1} \cdot W \cdot ENC}{\sum_{i=1}^n Q_i} \quad (4.2)$$

where  $W$  is the strip width,  $n$  is the number of strip involved and  $ENC$  is the system noise expressed as Equivalent Noise Charge.

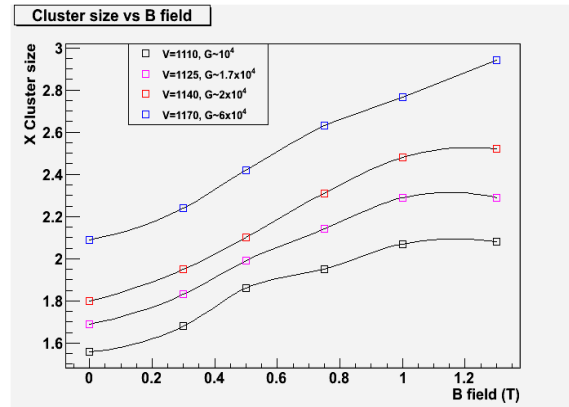


Figure 4.4: Cluster Charge Distribution with magnetic field and different gas gain (650 μm pitch)

In order to estimate the (ideal) spatial resolution achievable using the new detector the parameters shown in table 4.1 have been used, obtaining, for a m.i.p. crossing orthogonally the ionization gap, a total amount of charge collected on X (Y) strips

of about 18 fC and an ideal resolution of about 50  $\mu\text{m}$  (considering the strip width  $\simeq$  strip pitch). Of course, the achievable spatial resolution should account also for additional effects related to particles incident angles and apparatus magnetic field (as both effects increase the cluster size), presently not included in the above-mentioned measurements.

**Table 4.1:** Parameters used to estimate the achievable spatial resolution

Ionization gap	3 mm
Strip pitch	650 $\mu\text{m}$
Gas Mixture	Ar/CO <sub>2</sub> (70/30)
Gas Gain	8000
ENC	1 fC
Cluster Size	3

#### 4.3.1.1 Dynamic Range

With the working conditions shown in table 4.1, the estimated gain fluctuation should be  $\sim 8\%$  (rms) [?] and, thereby, the collected charge should range between  $\sim 13$  and  $\sim 23$  fC. Then, assuming a safety factor of 3 an upper limit for the delivered charge of about  $\sim 60$  fC can be inferred. On the other hand, also electronic noise could be lower than the 1 fC reported in table 4.1, Therefore a range between 0.5-60 fC can be set for the delivered charge.

#### 4.3.1.2 Resolution

To define the ADC number of bits required to correctly span the foreseen input charge range we can use the IEEE definition of eq. (4.3) for effective number of bits (ENOB)

$$ENOB = \log_2\left(\frac{FE_{I_{rms}}}{Qe_{rms}}\right) = \log_2\left(\frac{F}{\sqrt{12}e_{rms}}\right) \quad (4.3)$$

where Q is the ADC average code bin width, F is the full scale range and  $E_{I_{rms}}$  is the ideal rms error ( $E_{I_{rms}} = Q/\sqrt{12}$ ). Replacing F with 60 fC and  $e_{rms}$  with 0.5 fC, an ENOB value of 6 bits can be deduced to encode the collected charge.

#### 4.3.1.3 Linearity and gain errors

Usually, front-end (including analog to digital data conversion stages) linearity and gain errors requirements in gas detectors are not a major issue, because of the large fluctuation involved in gas gain. Anyway, as we are interested in detecting differences in the strip collected charge, both integral and

differential non linearity (INL and DNL) and gain errors should be lower than 1 LSB to correctly reconstruct the signal distribution shape over several strips.

### 4.3.2 Time Measurement Specifications

#### 4.3.2.1 Resolution

The time resolution of GEM based detectors has a strong dependence on the used gas mixture (the time resolution is mostly limited by the primary ionization in the first gas gap). Typical values range from  $\sigma_t \simeq 5$  ns (Ar/CF<sub>4</sub>/Iso = 65/28/7) and  $\sigma_t \simeq 10$  ns (Ar/CO<sub>2</sub> = 70/30) [?]. Because of the detector time resolution upper limit, the front-end time measurement specifications can be loosened up; for example a 2 ns contribution due to electronics worsens the achievable time resolution less than 10% for the Ar/CF<sub>4</sub>/Iso gas mixture (or less than 5%, if the Ar/CO<sub>2</sub> standard gas mixture is used).

#### 4.3.2.2 Dynamic range and linearity

The time dynamic range is mainly dominated by the electron drift velocity and the width of both ionization and transfer gaps. Anyway, whatever solution will be used for the ionization/transfer gaps spacing (3/2/2/2 or 3/1/2/1) and the gas mixture (7 cm/ $\mu\text{s}$  with 70/30 Ar/CO<sub>2</sub> or 11.5 cm/ $\mu\text{s}$  with 65/28/7 Ar/CF<sub>4</sub>/ISO – C<sub>4</sub>H<sub>10</sub>) the drift time will not be longer than 200 ns. Then, in order to have some redundancy, a time measurement range of 500 ns (compatible with the MDC drift time) could be used. According to the chosen full range, the integral non linearity for the time measurement should be lower than 2 ns.

### 4.3.3 Preamplifier Boards

Preamplifier boards will be located on the detector, then both dimensions and power consumption are issues that must be considered in the design. The board dimensions are mainly dominated by the strip connector and the preamplifier (ASIC) protection circuit, while the power consumption is strictly related to the ASIC circuit. Therefore, the single channel power consumption must be as lower as possible .

Furthermore, because the readout electrode will be implemented on Kapton foils, a suitable structure must be foreseen to allow safe insertion and extrac-

tion of the boards, in order to avoid kapton connection damage. Some details of the foreseen support structure and board are shown in Fig. 4.5

Each preamplifier boards will host two ASICs, 64 channels each one, for strips readout. The devices must provide a low sensitivity to the input capacitance (i.e. a series noise contribution of the order of 40 erms/pF), as well as good gain (of the order of 4-5 mV/fC in the head-stage preamplifier) and the capability to sustain the foreseen single channel rate.

Although, the wide spread of the input capacitance (due to the different V strips lengths) does not allow a fully optimization of the head/shaping stages, efforts have been devoted to minimize the readout electrode parasitics and, as a consequence, the parasitic spread. Because the strip capacitances are dominated by the two view cross-capacitance, a study has been carried out using Maxwell simulator to investigate the possibility of decreasing the coupling. Simulation result, shown in Sec. 2.2.2, points out that a clever geometry in strip design lead to a 30% reduction of the strip capacitances. A further critical point in the front-end chain design consist in the single strip input rate (signal + background). A high input rate would require a baseline restorer before the ASIC analog to digital conversion stage to limit the offset fluctuation and also deeper buffers in the readout boards then increasing the time required to find the event correct window.

As an estimation of the single strip maximum rate we take the value of 60 kHz/strip evaluated in section 1.2.

#### 4.3.4 The front-end ASIC

**COMMENT: Author(s): Rivetti**

The analog readout chosen for the BESIII CGEM-IT requires the development of a custom ASIC, in fact the GASTONE ASIC [?] used to instrument the KLOE-2 CGEM-IT cannot be used because delivers only a single bit information per strip. On the other hand analog chips such as APV25, used for instance for GEM readout [?] by COMPASS experiment, cannot be used because it is based on IBM 250 nm technology, which is not exportable to China. Taking advantage of the expertise of the Microelectronics Lab of Torino INFN Section, where several ASICs have been already designed and implemented [?, ?, ?, ?, ?], we have then opted for the development of a new ASIC suitable for CGEM-IT requirements. The UMC 110 nm technology will be

used as baseline, since the fully implemented chip can be exported to China.

The moderate charge resolution required by the GEM detector makes the use of the Time-over-Threshold (ToT) technique, already used in [?, ?], an attractive solution for data digitization.

A ToT system is very similar to a simple binary one and it consists of a front-end amplifier followed by a threshold comparator. The charge information is preserved by encoding the duration of the discriminator output pulse. When the signal crosses the threshold, the comparator fires and the corresponding time is captured by the digital logic and provides the event time-stamp. The trailing edge of the signal is also stored to allow to measure by difference the total pulse length.

By properly designing the analog circuitry, it is possible to maintain an adequate linearity. The ToT approach is thus particularly suited for circuits implemented in very deep submicron CMOS technologies, which operate with power supply voltages smaller than 1.5 V.

The time-base necessary to measure the signal duration can be obtained by counting the ticks of a reference clock. To meet the specification on the time resolution of the GEM system of the order of 1 ns, a clock of several hundreds MHz would be necessary. The use of such a high speed clock, although possible, entails several issues for what concerns its generation and propagation on chip and can lead to a power-hungry system. It appears thus preferable to use a slower clock, achieving the required time resolution by interpolation.

The front-end ASIC will have a modularity of 64 channels and it will be implemented in a 110 nm CMOS technology. Each channel features a front-end amplifier, optimized for the GEM detector, and a low-power time-to-digital converter, based on an already existing IP (Intellectual Property) block.

##### 4.3.4.1 The front-end amplifier

The large capacitance of the GEM detector ( $\sim 100$  pF) requires a careful design of the input stage to achieve the target noise level of 0.5 fC rms. A transconductance of 20 mS in the input transistor allows a in-band input impedance of about  $50 \Omega$  and a noise level of 2000 electrons already for a peaking time of 50 ns. Preliminary simulations in the chosen technology show that such performance can be achieved by putting  $900 \mu\text{A}$  in the input stage, which results in a power consumption of 1.1 mW. The first stage thus consists of a conventional charge

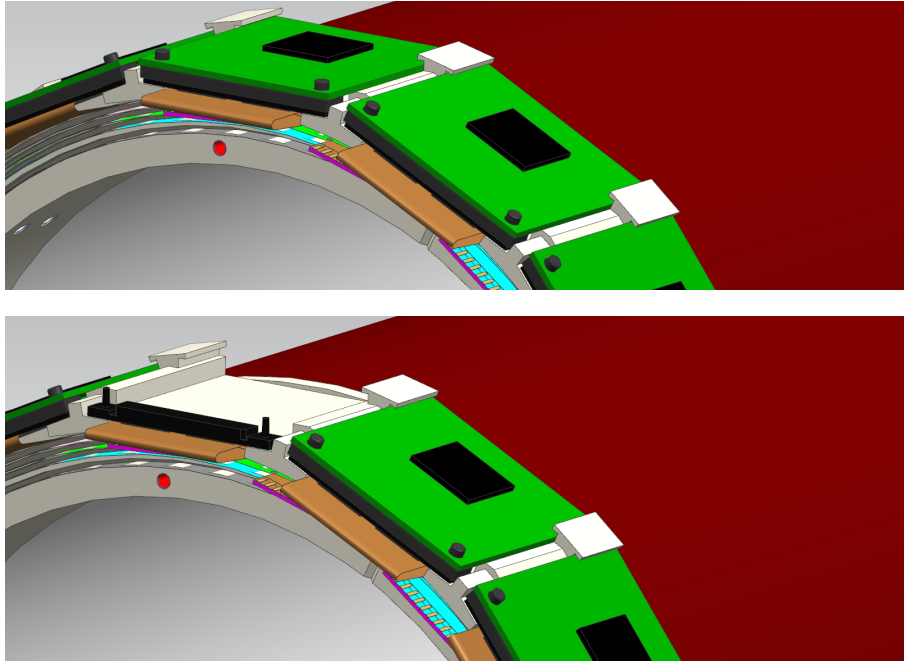


**Figure 4.5:** Preamplifier support structure

sensitive amplifier with active feedback network and pole-zero cancellation. The fast current signal is then filtered and processed by the ToT stage, which is basically an integrator with a constant current source as feedback. A low-power continuous-time-time discriminator compares the output of the ToT stage against a threshold which can be fine-tuned with a local Digital to Analog Converter (DAC), thus generating the digital output pulse with a length proportional to the integrated charge.

#### 4.3.4.2 The time encoder and data readout

A global counter counts the period of a reference clock and distributes a Gray-encoded word to all channels. When a hit is detected in the channel, the counter values is stored into local registers. A time interpolator is then triggered to measure the time elapsing between the hit and the next clock edge. Using a reference clock of 40 MHz and an interpolation factor of 64, a time bin of 390 ps results, which implies a digitization error of 110 ps.

This is already ten times smaller than the envisaged detector resolution. Based on previous implementation of the interpolator, it is expected that it will not take more than 1 mW per channel. The readout scheme will employ a data-push architecture. Any

event passing the selection threshold is digitized and queued for readout. Considering a maximum data rate of 60 kHz per channel and 32 bits per word, a maximum data rate of 120 Mbit/s per chip results. This can be easily accommodated by a single output LVDS link. The digital logic of the ASIC will be protected against Single Event Upset (SEU) by using Hamming encoding and error correction techniques.

## 4.4 Off-Detector Electronics

As already shown in Fig. 4.2 the Off-Detector Electronics is made of Readout Boards and Concentrators Boards. The boards will be hosted in custom crates located as near as possible to the detector, compatibly with background radiation as the boards will host several FPGAs.

### 4.4.1 Readout Boards

The Readout Boards will implement (together with the Concentrator Boards) the interface between the DAQ and the front-end electronics located on the detector. The main task of the boards is to match the data-driven (i.e. trigger-less) architecture of the

front-end boards with the existing BESIII DAQ architecture based on a Level 1 trigger and a  $6.4 \mu\text{s}$  latency time, then implementing the data flow shown in Fig. 4.6.

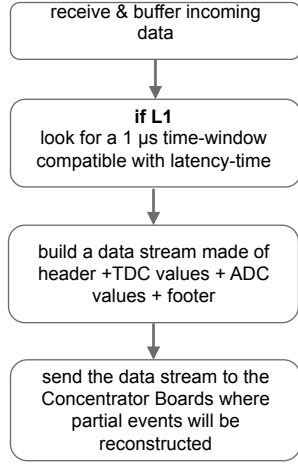


**Figure 4.6:** Readout Board data flow architecture

#### 4.4.1.1 Receiver Section

This section besides to match the electrical constraints of the front-end board data transmitter must include an adequate size buffer to store incoming events waiting for Level 1 trigger delivery. A rough estimation of the buffer size can be carried out from the foreseen single channel data rate ( $\sim 60 \text{ kHz}$ ) and event size ( $\sim 32 \text{ bits}$ ).

Because of the ASIC data pushing architecture and assuming that only the effective detected signals are transmitted (no noise counting) the number of foreseen events per second can be evaluated by multiplying the single channel data rate ( $\sim 60 \text{ kHz}$ ) by the number of channels (64), then obtaining  $3.84 \text{ MHz}$  effective background rate from output serial link, that is, in average, a 50 bits data packet about every  $0.26 \mu\text{s}$ . Then the pipeline should be able to keep 26 data packets (equation 4.4):

$$L = \frac{\text{Trigger Latency}}{\text{Background Rate Period}} + 1 = \frac{6.4 \mu\text{s}}{0.26 \mu\text{s}} + 1 = 26 \quad (4.4)$$

#### 4.4.1.2 Derandomizer Section

This section, specifically, implements the extraction of the data packet corresponding to the event validated by the L1 signal, as already shown in Fig.

4.6. Because of the readout geometry (the anode odd and even strips will be readout on different sides), no zero suppression or noise rejection can be implemented in this section.

### 4.4.2 Concentrator Boards

As data concentrator boards, VME64x readout modules called ATLB, shown in Fig. 4.7, can be used [?, ?]. The devices, which were developed at the Uppsala University and used in various experiments including the KLOE-2 Inner Tracker, feature 16 optical interfaces (SFP) receiving/transmitting data at  $2 \text{ Gb/s}$ . Depending on the implemented firmware, the ATLB can be used for evaluating trigger decisions, event formatting and as a general DAQ unit. The received data are stored in 16 individual FIFO buffers of up to  $32 \text{ kB}$  capacity. After merging, the output data are read out over a VME bus, while the device supports the full range of VME64x/VXS protocols, including BLT ( $40 \text{ MB/s}$ ), MBLT ( $80 \text{ MB/s}$ ), 2eVME ( $160 \text{ MB/s}$ ), 2eSST ( $320 \text{ MB/s}$ ) and VXS ( $3.2 \text{ GB/s}$ ). For readout continuity, a  $2 \text{ MB}$  output FIFO is provided.

For control/diagnostic purposes the ATLB utilizes a MicroBlaze™ based embedded system with  $64 \text{ MB}$  of DDR RAM,  $8 \text{ MB}$  of Flash ROM, USB and 10/100 Ethernet as peripherals. The ATLB board is based on Virtex-5 FPGAs from Xilinx, built in  $65 \text{ nm}$  technology.

A follow-up development of the readout board utilizing the newest Xilinx 20/22 nm technology Kintex-7/ZYNQ-7 has been started. The new module will act as a stand-alone device and feature 16 optical interfaces of up to  $12.5 \text{ Gbit/s}$ , while the output data communication is planned over a  $1 \text{ Gbit}$  Ethernet, saving on the costs of crates and crate controllers. An embedded ARM9 processor system will support all necessary remote control functions.

## References

- [1] KLOE-2: F. Archilli et al. Technical Design Report of the Inner Tracker for the KLOE-2 experiment. Technical report, 2010.
- [2] R. Debbe, J. Fischer, D. Lissauer, T. Ludlam, D. Makowiecki, et al. A Study of wire chambers with highly segmented cathode pad readout for high multiplicity charged particle detection. *IEEE Trans.Nucl.Sci.*, 37:88–94, 1990.
- [3] B. Ketzer, M.C. Altunbas, K. Dehmelt, J. Ehlers, J. Friedrich, et al. Triple GEM

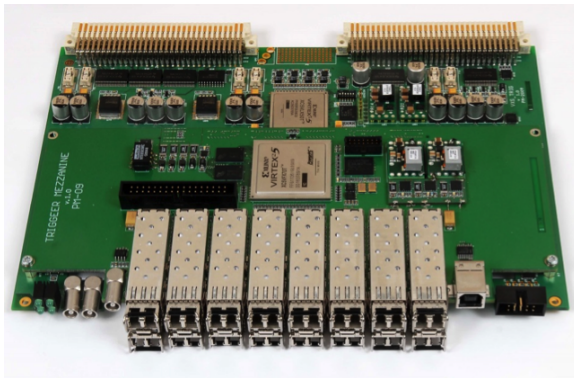


**Figure 4.7:** VME64x ATLB

tracking detectors for COMPASS. *IEEE Trans.Nucl.Sci.*, 49:2403–2410, 2002.

- [4] G. Bencivenni, P. De Simone, F. Murtas, M. Poli-Lener, W. Bonivento, et al. Performance of a triple-GEM detector for high rate charged particle triggering. *Nucl.Instrum.Meth.*, A494:156–162, 2002.
- [5] A. Balla, G. Bencivenni, P. Branchini, A. Budano, S. Cerioni, et al. GASTONE64: A new front-end ASIC for the cylindrical GEM Inner Tracker of KLOE-2 experiment at *DAΦFNE*. *Nucl.Instrum.Meth.*, A732:523–525, 2013.
- [6] B. Ketzer, S. Bachmann, M. Capeans, M. Deutel, J. Friedrich, et al. GEM detectors for COMPASS. *IEEE Trans.Nucl.Sci.*, 48:1065–1069, 2001.
- [7] A. La Rosa, F. Marchetto, J. Pardo, M. Donetti, A. Attili, F. Bourhaleb, R. Cirio, M.A. Garella, S. Giordanengo, N. Givehchi, S. Iliescu, G. Mazza, A. Pecka, C. Peroni, and G. Pittà. Ionizing radiation effects on a 64-channel charge measurement ASIC designed in CMOS 0.35- $\mu\text{m}$  technology. *Nucl.Instrum.Meth.*, A593:619–623, 2008.
- [8] G. Dellacasa, S. Garbolino, F. Marchetto, S. Martoiu, G. Mazza, et al. A 130-nm ASIC prototype for the NA62 Gigatracker readout. *Nucl.Instrum.Meth.*, A650:115–119, 2011.
- [9] G. Mazza, D. Calvo, P. De Remigis, T. Kugathasan, M. Mignone, et al. A CMOS 0.13- $\mu\text{m}$  silicon pixel detector readout ASIC for the PANDA experiment. *JINST*, 7:C02015, 2012.
- [10] M.D. Rolo, R. Bugalho, F. Goncalves, G. Mazza, A. Rivetti, J.C. Silva, R. Silva, and J. Varela. TOFPET ASIC for PET applications. *JINST*, 8(02):C02050, 2013.
- [11] A. Goerres, R. Bugalho, A. Di Francesco, C. Gastón, F. Goncalves, et al. A free-running, time-based readout method for particle detectors. *JINST*, 9:C03025, 2014.
- [12] P. Branchini, A. Budano, A. Balla, M. Beretta, P. Ciambrone, et al. Front-end DAQ strategy and implementation for the KLOE-2 experiment. *JINST*, 8:T04004, 2013.
- [13] P. Marciniewski, P. Plucinski, K. Fransson, L. Heijkenskojld, A. Kupsc, et al. A Trigger System based on fast sampling ADCs - implementation and tests. *IEEE Nucl.Sci.Symp.Conf.Rec.*, 2011:38–42, 2011.



## 5 DAQ and Trigger

---

**COMMENT: Author(s): Zhenan LIU, Xiaolu JI**

### 5.1 Requirements

The CGEM DAQ system should be integrated into the current BESIII DAQ framework, in order to work synchronized with other detectors. Same as for other systems in BESIII, DAQ system will provide the basic functions like configuration, data taking, checking, assembly and data storage. Besides that, DAQ will support real-time histogram display, error reporting, and other assistant features.

BESIII DAQ system can be separated into two parts, front-end and back-end.

The front-end DAQ sub-system is the interactive interface of DAQ system with electronics, trigger and detector systems. The most important purpose of front-end DAQ system is to read data fragments from electronics modules. In current BESIII electronics design, the electronics modules of different detector systems are all designed in VME standard. All the data streams are transferred by VME bus. Motorola MVME5100 is adopted as the system controller to achieve all the functions which should be implemented by frontend DAQ sub-system.

The back-end sub-system of BESIII DAQ is designed to do the event building, event filter, data storage, run control and monitor, online histogram display and so on. The BESIII DAQ back-end system is a universal framework which provides essentially the 'glue' that holds the various sub-systems together. It does not contain any elements that are detector specific, and all the functions and devices are configurable for expert users. So the CGEM-IT can be easily integrated to the current system framework.

The existing inner drift chamber is not used in the BESIII trigger system for trigger track finding, so there is not easy and direct way to combine the CGEM-IT into present trigger system. Future consideration could be thought based on the results of detector simulation with good understanding of the CGEM. So the requirement to the present hardware (level 1) trigger system is that, to upgrade the fast control motherboard for trigger distribution to provide another fast control link to CGEM sub-system to move out the corresponding data stored in FEE

pipeline buffer to readout buffer for readout.

### 5.2 Bandwidth

From the previous chapters, the total amount of the CGEM on-detector electronics channels is about 10,000. And the BESIII trigger rate is designed to the maximum 4 kHz frequency. Suppose each single channel event contains 32bits data, for the extreme case, when 100% channels fired, the whole bandwidth could reach 1.3 Gbps ( $10,000 \times 4,000 \times 32$ ). Besides that, the basic data structures like event header and footer will make the DAQ input data bandwidth even higher. As shown in Chapter 5, the data concentrator boards will use the 1Gbit Ethernet to transmit data to DAQ. The current BESIII DAQ system is a distributed system, which means the data streams can be processed at different machines, so the BESIII DAQ can handle the data bandwidth by deploying more blade servers.

### 5.3 Storage

In BESIII DAQ, the data fragments from each detectors will be packed into a full event by the uniform trigger ID. SFO (sub-farm output) component in DAQ system will save these full events together with some important run informations into the raw data files. Then the raw data files will be sent through Ethernet to the clusters of IHEP computing center for permanent storage.

There is no need to the storage for trigger system.



## 6 Integration of the CGEM-IT with the Spectrometer

---

**COMMENT: Author(s): Savrie', Felici, Qun, Marcello**

### 6.1 Interfacing Mechanical Design

**COMMENT: Author(s): Cibinetto**

The CGEM-IT must interface internally with the beam pipe and externally with the outer drift chamber; in addition the beam support flanges limit the available space at the edges. Fig. 6.1 shows a section of the BESIII interaction region: only the layer 2 is designed with full level of details, for layer 1 and layer 3 just the expected volume is displayed.

On the inner side, the beam pipe design includes the cooling system, while on the external side only the carbon fiber cylinder is displayed. On the two sides there are only the two main steel flanges which support the beam pipe. In order to hold the CGEM-IT and the carbon fiber cylinder, additional flanges need to be added in the available space.

The inner drift chamber removal and the installation of the CGEM-IT will be performed after the removal of the beampipe. After the removal of inner drift chamber, the carbon fiber cylinder will be installed and glued to the outer chamber. Then the fully cabled CGEM-IT will be inserted with proper mechanical tooling that will be developed ad hoc in order to avoid mechanical interferences.

Gas lines, high voltage and signal cables will be grouped in bundles and will follow the same path of the old drift chamber cables. The space needed for the cables and utilities is under evaluation.

### 6.2 HV Systems

**COMMENT: Author(s): Giulietto FELICI, Christoph Rosner**

#### 6.2.1 Requirements

Despite the triple GEM structure allows to archive a gain of the order of  $10^4$  with a negligible discharge

propagation probability, the use of a design including an adequate factor of safety is mandatory for a detector that will be not accessible after installation. Moreover, a robust HV distribution design simplifies the ASIC readout protection network design, a not negligible point in a design where read-out board sizes must be reduced as much as possible.

Because the discharge propagation is a function of both the induction field value and the GEM capacitance, two rules can be adopted in order to decrease the probability of discharge propagation: operate at low induction fields (less than 5 kV/cm) and/or segment the lower GEM electrode in order to reduce its capacitance.

In the Inner Tracker design both rules have been adopted. Firstly, the detector has been design to operate with the induction field well below the 5 kV/cm limit still maintaining a good efficiency and, secondly, the upper electrode of each GEM has been segmented to reduce the capacitance involved in the discharge.

An example of electrode segmentation is shown in Fig. 6.2. Each lower layer is divided in macro-sectors while the corresponding upper layer is further divided in 10 sub-sectors then limiting the capacitance involved in case of discharge. The number of macro/micro sectors used in the IT design, as well as the micro-sector capacitance, are shown in table 6.1

#### 6.2.2 Overall Design

The HV distribution system, consists of four parts: the main HV system, the HV meter, the HV distributor and, finally, the cables and the custom HV connectors. The adopted partition allows to limit the number of main HV channels of each layer to 7, then simplifying the implementation of a reliable system (in case of single CGEM problem all the layer voltages must be turned off with the appropriate ramping down procedure), monitor the CGEM currents and easily disconnecting in case of damaged micro-sectors.

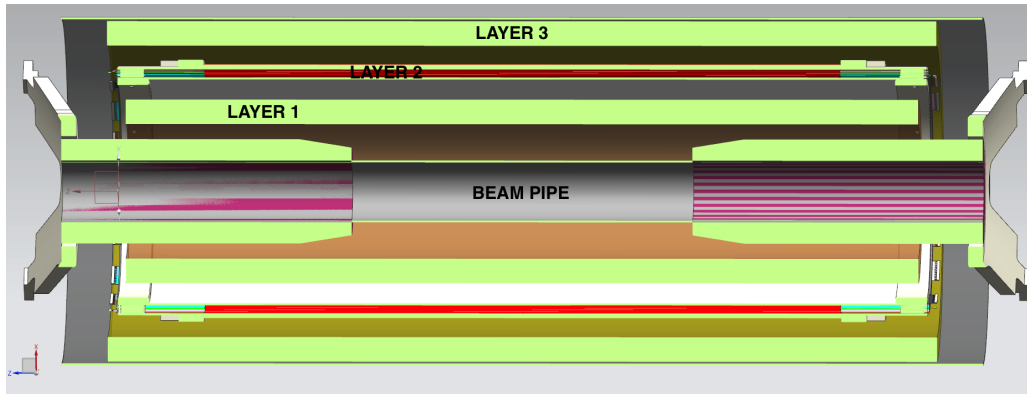


**Figure 6.1:** A side section of the CGEM-IT around the beam pipe. Only the layer 2 is designed with full level of details.

**Table 6.1:** Number of HV macro-sectors/micro-sectors per layer and relative parasitic capacitance

layer (single CGEM)	macro-sectors	micro-sectors	micro-sector capacitances
1	4	40	4.6 nF
2	8	80	4.3 nF
3	12	120	2.9 nF

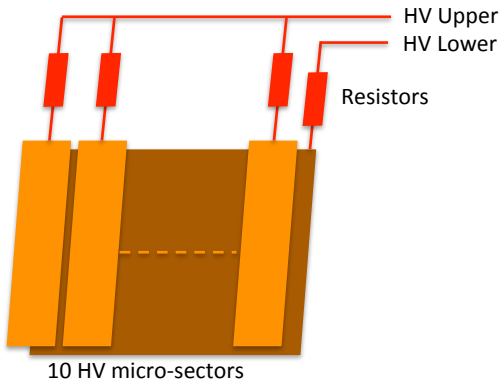


**Figure 6.2:** HV segmentation to reduce GEM capacitance in case of discharge

A block diagram of the system<sup>1</sup> is shown in Fig. 6.3. It is made of:

1. A main power supply section to generate the cathode and the 6 triple GEM voltages;
2. A Current Monitor to sense CGEMs dragged currents;
3. Distribution Boxes to route the main voltage to the micro-sectors;
4. Cables and custom connectors.

### 6.2.3 Connectors and cables

Three types of connectors and two types of cables will be used in the system. RG59 high voltage cables together with SHV connectors will connect the HV power supply to the current meter while multi-pin connectors and multi-core cables will be used to interconnect the current meters to the distribution boxes. Finally, multi-core cables together with custom connectors will deliver the high voltage to the detector. The custom connector will host a 10 M $\Omega$  resistor (micro-sectors) and 1 M $\Omega$  (macro-sectors) for current limitation purpose (see fig. 6.3).

### 6.2.4 Distribution Boxes

Two distribution boxes per layer (one each detector side) will be used to supply HV (6 distributors for the full detector). For example Fig. 6.4 shows the details of the HV chain used for the third layer.

Each CGEM of the third layer is made of 12 macro-sectors for a total amount of 120 micro-sectors per CGEM. Macro-sectors will be distributed on both detector side, giving a total amount of 6 macro-sectors (and 60 micro-sector) per side. Each single cable and custom connector will host only voltages for a CGEM sector then limiting the voltage differences in the custom connector to less

<sup>1</sup> The Cylindrical GEM detector for the KLOE-2 Inner Tracker - G. Morello

**Table 6.2:** HV distribution system summary

component	Number	Size	Power Requirements
HV mainframe	1	19" - 8U	4 kW (max)
HV boards (12 channels)	3		
Current Monitor	1	19" - 2U	800 W
HV distribution boxes	6	19" - 2U	
Multi-core (14) HV cables	33/side	~ 10 mm diameter/cable	

than 500 V. Cathode connections will be routed by means of dedicated cables/connectors, because of the voltage required to supply the electrode ( $\sim 4$  kV).

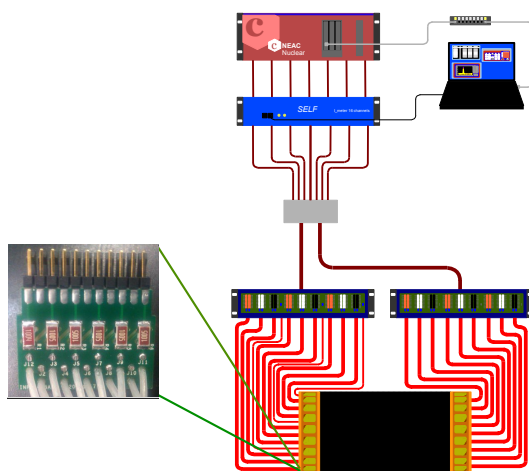
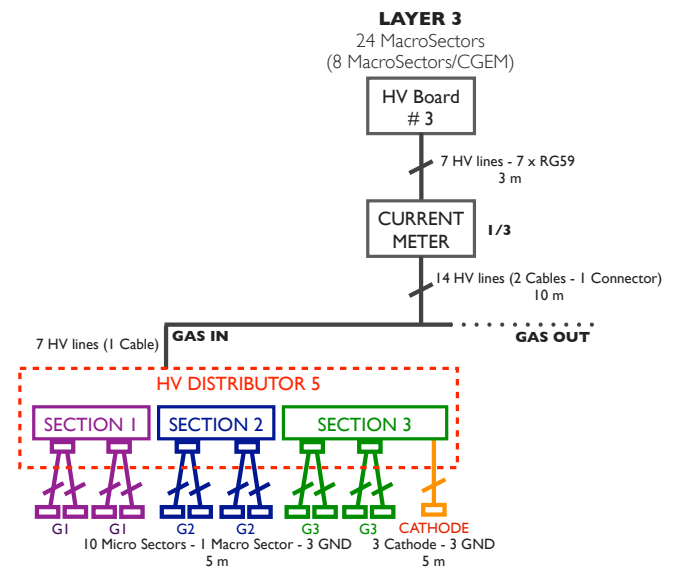
### 6.2.5 HV summary

Table 6.2 shows the space and power requirements of the high voltage distribution systems, as well as the number (and size) of cables entering the detector.

## 6.3 Slow Controls

**COMMENT: Author(s): Mei YE**

The detector control system (DCS) that monitors the environmental parameters and the performance of spectrometer and accelerator is critical for BE-SIII operation. The DCS consists of six subsystems that monitor thousands of sensors distributed

**Figure 6.3:** Single layer HV distribution block diagram**Figure 6.4:** High voltage distribution chain connection example

throughout the spectrometer and detector hall. Critical parameters such as environmental temperature, humidity and radiation levels are monitored in real time. The system also reads the monitoring outputs of thousands of hardware devices and reports the device status, voltages, current and other parameters. The DCS controls and monitors the detector high voltage system. The DCS also controls and monitors the gas systems and provides safety interlocking among detector systems and between detector and accelerator.

The DCS is organized into the front-end layer, local control layer and global control layer (GCL). A LabVIEW based software framework is used for the data collection control. Data of approximately 9000 readouts are recorded once every 10 s. Network communication and web server technologies are used for the data collection and GCL.



## 7 Simulation of Cylindrical GEM Inner Tracker

**COMMENT: Author(s): Calcaterra, Cibinetto, Maggiora, Liangliang**

### 7.1 Parametric Simulations

**COMMENT: Author(s): Liangliang**

#### 7.1.1 Digitization and Cluster Model

**COMMENT: Author(s): Gianluigi CIBINETTO, M. Destefanis, Linghui Wu**

When a charged particle passes through the drift area ionization occurs. Electrons produced by ionization drift in the electric field, and signals are induced in the anode plane. During the drift, the presence of a strong magnetic field and electron diffusion modify the drift properties and have impact on the charge distribution in the anode plane [?], as shown in Fig. 7.1.

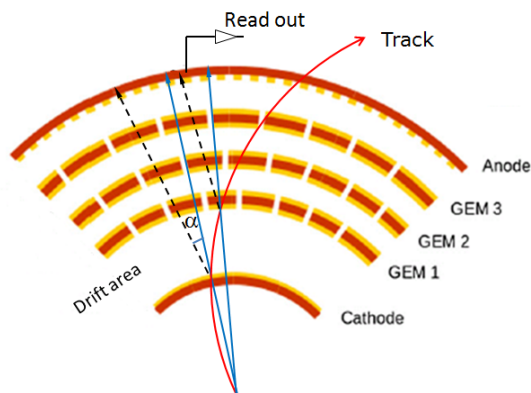


**Figure 7.1:** Diagram of digitization with (blue solid lines) and without (black dashed lines) taking into account the Lorentz angle  $\alpha$  and electron diffusion.

Due to the absence of drift parameters, the present simulation software adopts a simple digitization model without taking into account the Lorentz angle  $\alpha$  (see Fig. 7.1) and electron diffusion. The track trajectory in the drift area, which is defined as sensitive volume, is propagated by several steps in Geant4. The energy loss, the momentum of the particle, the position of the starting and ending point in each step can be recorded. At the end of this process all the steps are summed in order to calculate the total energy loss by the particle and its

entrance and exit points. The registered positions are then projected to the anode plane, where the signals are supposed to be registered, as shown in Fig. 7.1. At this level, from those positions the identification numbers of the fired strips are extracted. The energy deposited in the sensitive volume is divided by the total number of fired strips, and it is equally shared among them.

In order to deliver a better simulation of the detector behavior, we developed a routine which considers a flat distribution of the deposited charge from the entrance to the exit point, already on the anode plane. The total energy is divided by 2, since at the anode we collect the signals on two strips planes ( $X$  and  $V$ ), and it is multiplied by the expected gain. The full amplification process should deliver charges of about 18 fC, which means 9 fC per readout plane. The gain is now fixed at 20000, but we expect a better estimation after the tests which are planned on a planar GEM prototype in the near future at the cosmic ray setup described in section 2.2.4. To calculate the collected energy, the charge distribution is integrated for each hit strip taking into account the entrance and the exit position of the track. Each strip number is, then, saved with the corresponding deposited energy value and stored in the CGEM “hit collection”.

A further improvement can be performed at the level of the event reconstruction process. At this stage we have the hits and the corresponding collected charges. For each hit one can smear the deposited energy by a Gaussian distribution along the two different readout coordinates, using the sigma value typical of each view. The obtained distributions are, then, integrated in order to obtain the signal contribution of each single strip. The described routine has been already prepared and needs to be implemented and tested within the reconstruction software. Before implementing the new digitization, precise indications about the CGEM deposited energy signal shape, that will be available with the upcoming tests on the CGEM planar prototype and Garfield simulations, are necessary. The obtained shape will be implemented in the described routines to increase the detail level of our simulation software. The modular structure of the described routines will allow an easy implementation of the charge distribution shape inside the already existing code.

Minimum thresholds on the collected charge are al-

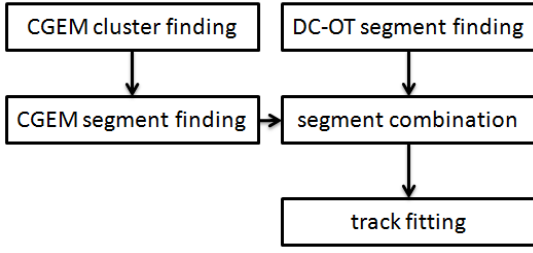


**Figure 7.2:** The flow diagram for the track reconstruction with CGEM-IT and DC-OT.

ready implemented and can be used in order to obtain a better simulation of the detector response. At present there is no lower limit to the collected charge of a registered signal, but we expect to be able to register deposited charges of about 1 fC.

## 7.2 CGEM-IT Full Offline Reconstruction

**COMMENT: Author(s): Liangliang**

The software packages for the full reconstruction are under development with the full simulation of the CGEM-IT and the DC-OT (drift-chamber-outer-tracker). The complete reconstruction procedure of charged tracks with this tracking detector configuration is designed to include the following items:

1. Cluster reconstruction with fired strips of CGEM
2. Track segment finding within CGEM-IT
3. Track segment finding within DC-OT
4. Combination of track segments
5. Track fitting based on Kalman Filter method

The corresponding flow diagram is shown in Fig. 7.2.

Due to the time limitation, the development for the second item is not started yet. So the track reconstruction procedure is simplified as a preliminary alternative, which is shown in Figure 7.3. So this section will focus on the introduction to the preliminary cluster reconstruction with fired strips of CGEM, track segment finding within DC-OT, the combination of segments within DC-OT and track fitting based on Kalman Filter method.

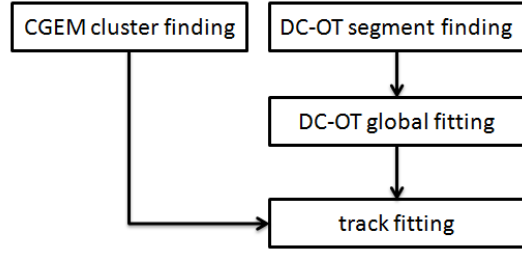


**Figure 7.3:** The flow diagram for the preliminary track reconstruction with CGEM-IT and DC-OT.

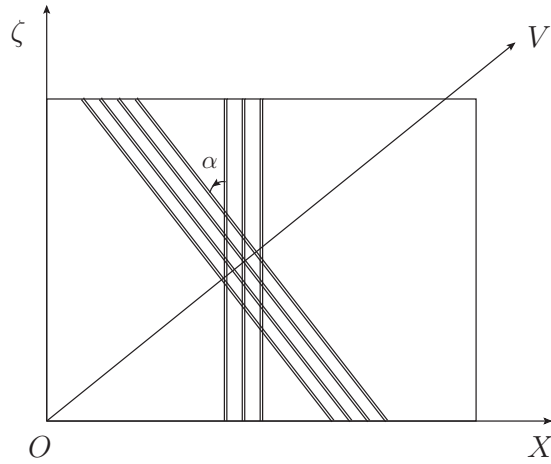


**Figure 7.4:** Schematic of one cluster induced by a charged track, composed of 3 X-strips and 4 V-strips on an unrolled CGEM plane, where the stereo angle  $\alpha$  is the opening angle between X-strip and V-strip, the X axis is perpendicular to X-strips, the V axis is perpendicular to V-strips and the  $\zeta$  axis is parallel to X-strips.

### 7.2.1 Cluster Reconstruction for CGEM

**COMMENT: Author(s): Liangliang**

When one charged track impacts CGEM, usually a set of X strips and V strips on the readout layer can gather some charge. The demonstration of one cluster on an unrolled CGEM is shown in Fig. 7.4.

A package named *CgemClusterCreate* is developed to do the cluster reconstruction. First, sets of continuous fired strips in X and V directions are found which are called X-clusters and V-clusters separately. Second, the possible intersections between X-clusters and V-clusters are found which are called XV-clusters. As a digital readout model is implemented in the simulation, the position in X (V) of each cluster is obtained by averaging the middle po-

sitions of the fired strips which compose this cluster:

$$X = \sum_{i=1}^{N_X} X_i / N_X$$

$$V = \sum_{i=1}^{N_V} V_i / N_V$$

where  $i$  is the index of strips,  $X_i$  ( $V_i$ ) is the middle position of strip  $i$  and  $N_X$  ( $N_V$ ) is the number of fired X-strips (V-strips). The corresponding position in  $\zeta$  is calculated by

$$\zeta = (V - X \cos \alpha) / \sin \alpha. \quad (7.1)$$

The position where the track impact the CGEM in the drift layer is obtained by the reconstructed position of the cluster with some necessary correction which depends on the model of digitization. An output data model, which is defined by a class named *RecCgemCluster*, contains the following information: layer ID, GEM ID, cluster type (X, V or XV) and position.

The obtained residuals in X and V from the cluster reconstruction for a MC sample of single 1 GeV/ $c$   $\mu^-$  tracks are shown in Fig. 7.5, which corresponds to a resolution 170  $\mu\text{m}$  in X and 575  $\mu\text{m}$  in V accordingly to the digital readout that is simulated.

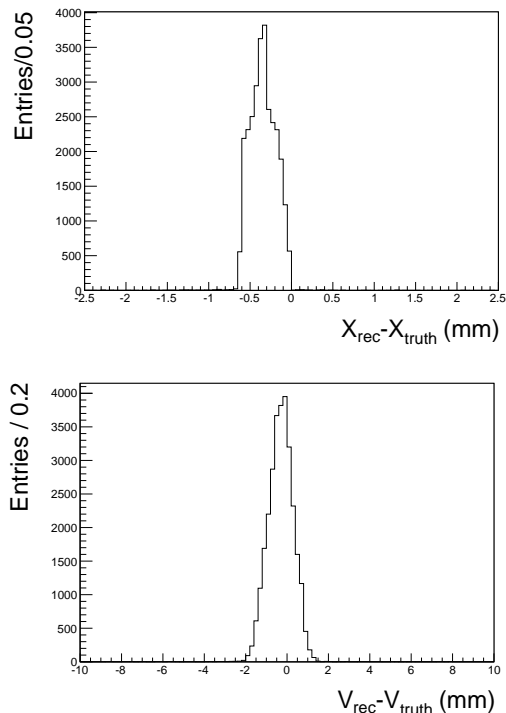


**Figure 7.5:** The position residuals in X(top) and in V(bottom) of the cluster for a MC sample of single 1 GeV/ $c$   $\mu^-$  tracks.

## 7.2.2 Track finding with the Drift-Chamber-Outer-Tracker

**COMMENT: Author(s): Yao ZHANG**

The DC-OT consists of 8 super-layers each of which consists of 3 or 4 signal layers. In the *MdcPatRec* algorithm, a series of hits of a charged particle in a super-layer are defined as a segment. The fired wire distribution of a segment in a super-layer is defined as a segment pattern. Segment patterns are collected to build a segment pattern dictionary. Every group of 8 signal wires in super-layers called segment neighbor wires, the relative position of segment neighbor wires is represented by the 8 wires marked by a cross in Fig. 7.6. A segment finder will match hits in each neighbor wires with the segment pattern in dictionary to find segments in all super-layers. After segment finding the axial super-layers segments with similar azimuth angle and radius will be assembled into circle tracks followed by a least square circle fit. Therefore, stereo segments can be added to circle tracks to constitute helix tracks and apply a global helix fit. After the global helix fit, tracks are reconstructed, and they are stored for the Kalman filter based fitting.

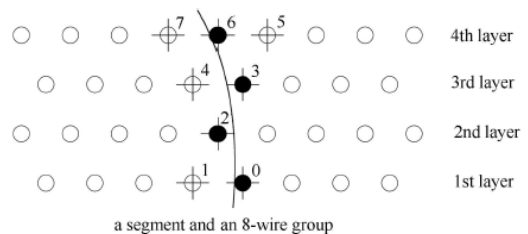


**Figure 7.6:** A schematic plot for illustrating a segment and an 8-wire group. The 4 layers of circles denote the signal wires in one super-layer. The arc shows a track, and the black solid circles are the fired wires of the particle. The 8 adjacent signal wires marked with a cross compose an 8-wire group used to match the segment pattern in segment finding.

The performance for the track finding with DC-OT is studied. To be compared with the situation with the full MDC (DC-IT and DC-OT), the ratios of the tracking efficiency for Bhabha events with DC-OT and the one with the full MDC are shown in Fig. 7.7. One can find that the tracking efficiency for barrel Bhabha events will not be affected, while the one for end-cap Bhabha events drops about 20% and drops rapidly when the  $\cos \vartheta$  is greater than 0.9.

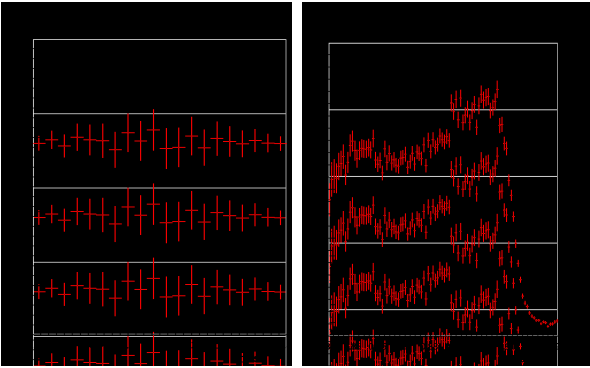


**Figure 7.7:** The ratio of the tracking efficiency with DC-OT only over the one with full MDC as a function of dip angle for barrel (left) and end-cap (right) Bhabha events.

### 7.2.3 Track fitting

The track fitting is based on the Kalman Filter method, which is performed by processing all the DC hits and the CGEM clusters belonging to a track in sequence. The basic steps of the track fitting with Kalman Filter include track parameters prediction, filter of the hit (cluster) and update of the track parameters, in which the following effects are considered: inhomogeneous magnetic field, energy loss and multiple Coulomb scattering. As the track segment finding in CGEM is currently not ready, the track fitting will process the DC-OT hits first. Then the CGEM clusters are directly added or rejected in the track fitting step. The association of the good cluster candidates to the DC-OT track is performed by minimization of the track fitting quality and imposing selections on the  $\chi^2$  fit. An optimization of the Kalman Filter track fitting is currently in progress.

## 7.3 Monte Carlo Simulation

**COMMENT: Author(s): Baldini, Maggiora**

An investigation of the new experimental scenario, in which the Inner Tracker of the BESIII spectrometer has been upgraded with the CGEM-IT, will be possible only when the tough and long job of developing a specific simulation and reconstruction framework for the CGEM-IT will be completed, and the full pattern recognition and tracking will be included in BOSS.

The benchmark channels to be considered are in particular those with final states including short liv-

ing particles; better capabilities in secondary vertices reconstruction (in particular in the  $rz$  view) will be in fact a natural consequence of the layout foreseen for the CGEM-IT anode readout (see Sec 3.1).

A first preliminary evaluation of such an exploit has been performed by the mean of a toy Monte Carlo simulation including the main features of the DC-IT and of the CGEM-IT, and in particular their different layouts and their stereo angles.

Two physics cases have been considered for the time being: the reconstruction of the secondary vertices corresponding to  $K_S^0$  and  $\Lambda$  charged decay modes, generated isotropically into the MDC fiducial volume (i.e.  $|\cos\theta| < 0.94$ ). Multiple scattering is affecting both cases in the same way, in a first approximation. In spite of the fact that DC-IT and CGEM-IT resolutions are almost the same in the  $r\phi$  view, the improvement in the overall vertex reconstruction is between a factor of 2 and a factor of 3, depending on the decaying particle and its momentum, as it is shown in Fig. 7.8.

The longitudinal position of the reaction vertex of the event is hence determined considering other charged tracks emerging from the collision point; also in this case our exercise suggests a better resolution, mainly due to the better measurement in the  $rz$  view. The significance of such an improvement depends on the considered process, and is currently under investigation. A more complete and detailed investigation will be performed as well with the full pattern recognition and tracking, when available.

A mild improvement, at a per mille level, is expected also in the total momentum resolution, coming from a better evaluation of the transverse momentum, which is measured by the curvature in the transverse view, and from a better evaluation of the longitudinal momentum, depending on the  $rz$  coordinates of the track hits.

## References

- [1] F. Sauli. Principles of Operation of Multiwire Proportional and Drift Chambers. *CERN Yellow Book*, 77-09, 1997.

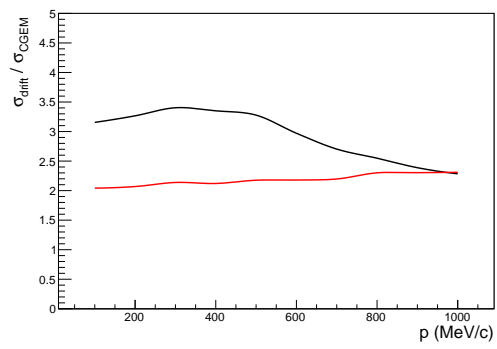


**Figure 7.8:** Ratio of the resolutions with which the secondary vertices corresponding to  $\Lambda$  (red line) and  $K_S^0$  (black line) charge mode decays are reconstructed by the DC-IT and the CGEM-IT.



## 8 Tasks and Plans

---

**COMMENT: Author(s): Maggiora, Calcaterra, Cibinetto, Marcello, Felici, Qun**

To build, deploy and commission the BESIII CGEM-IT in IHEP within the end of 2017 is certainly challenging.

This chapter offers a summary, an overview of the current picture for the tasks needed to achieve such a goal, and for their sharing among the different Institutions that constitute the Community that has aggregated within BESIII on the CGEM-IT project: Ferrara, Frascati and Turin for INFN, the different groups from the Helmholtz-Institut and the University in Mainz, Uppsala and, of course, IHEP. The current schedule and the current achievements are shown.

Manpower and (direct and indirect) funding issues will also be addressed.

### 8.1 Tasks

#### 8.1.1 CGEM-IT design

The CGEM-IT must be inserted inside the existing BESIII Outer DC BESIII, taking the place of the deteriorating DC-IT. The design of the BESIII CGEM-IT takes inspiration from the design of the KLOE-2 CGEM-IT, taking advantage from the gained experience, but trying also to reduce the amount of dead material in the vertex region of the spectrometer. In order to reduce the amount of dead material, three GEM planes are foreseen, with Rohacell supports and a new anode design. The Maxwell software is being used to investigate the different anode strips' configurations, while the Garfield software is being used for the charge sharing studies needed for the analogue readout.

A planar prototype has been assembled in Frascati and will be used to test the new anode design before proceeding to order of the anode foils for the full CGEM-IT; the planar prototype will allow also to optimise the gas mixtures to be fluxed in the CGEM-IT.

The mechanical design of the new detector must take into account the several challenging constraints introduced by the already existing spectrometer and by the reduced space available. The middle layer of the CGEM-IT will be almost completed in

the early 2015. Both the anode and the cathode will be designed by INFN personnel and hence produced at CERN.

The procedure of the insertion of the CGEM-IT in the existing Outer DC is far from being trivial, and its definition will require significant efforts and manpower, and an effective knowledge transfer from IHEP to INFN experts. Once the design and the insertion procedure have been defined, proper tooling for the construction and the insertion of the CGEM-IT must be designed and built, modifying the tools still available from KLOE-2.

The different sub-tasks of the current task are described herewith.

##### 8.1.1.1 Design of the mechanical structure of the detector (INFN)

The design of the mechanical structure has been and will be performed in Ferrara in collaboration with Frascati, within the layout inspired by the KLOE-2 CGEM-IT, but being adapted to the constraints introduced by the BESIII Outer DC, by the new BESIII FEE, and by the new Rohacell supports adopted to reduce the total radiation length. A continuous interaction and knowledge transfer from IHEP on the existing BESIII spectrometer is needed.

The design of the mechanical structure of the middle layer has been completed and used to procure molds and gem foils for the first layers, and to design the needed modification to the assembly tools in Frascati.

##### 8.1.1.2 Design of the GEM foils and of the cathode for each of three layers of the IT (INFN)

The design has been and will be performed in Ferrara, profiting of the experience of Frascati experts involved in the construction of the KLOE-2 CGEM-IT and of the interaction with Rui Olivera at CERN. The design of the components for the middle layer has been completed and the corresponding material procured.

### **8.1.1.3 Design and eventually further optimisation of the anode for the layers of the IT (INFN)**

The anode readout adopted by KLOE-2 cannot be produced anymore by CERN, due to very low efficiency of the manufacturing procedure. The investigation of an alternative layout of the anode w.r.t. standard readouts, the only option left on the market, has been a task shared among Ferrara and Frascati experts. The corresponding design will be soon finalised, leading to a significant improvement of the signal quality w.r.t. the standard readout; as a backup option, once the test of the new anode will be performed in the planar setup, we could revert to the standard (COMPASS like) strip readout.

### **8.1.1.4 Integration of the Inner Tracker with the existing BESIII spectrometer (INFN and IHEP)**

The CGEM-IT has to be integrated with the existing BESIII spectrometer. This task, performed by Ferrara and Frascati people, also depends on a continuous knowledge transfer from IHEP experts. It relies also on the cooperation of people from Ferrara, Frascati and Torino with the Mainz people developing the HV system and the Uppsala and INFN people developing the electronics.

While the mechanical design of the middle layer has already been performed in order to grant an effective integration, more work is needed in this task as far as the inner and the outer layer are concerned.

### **8.1.1.5 Define the installation procedure (including the insertion in the existing Outer Drift Chamber) and test on mockup (INFN and IHEP)**

A challenging procedure has to be defined to insert the CGEM-IT in the BESIII Outer DC. IHEP people must face a very similar challenge defining the insertion procedure for the new DC-IT being built. The former could inherit many aspects from the latter, although several changes must be expected. The insertion procedure could also be tested making use of the mockup provided by IHEP.

### **8.1.1.6 Production or modification and test of the tooling needed for detector construction (INFN)**

The tooling originally used to construct the KLOE-2 CGEM-IT are still available in Frascati, but the

BESIII CGEM-IT geometry is different (starting from the length of the three layers and their radius, different from KLOE-2 ones); the tooling needed for the CGEM-IT construction must be modified and tested by Frascati experts.

### **8.1.1.7 Production and test of the installation tooling (INFN and IHEP)**

The installation procedure, in particular the insertion in the BESIII Outer DC, requires specific tooling, that may partially inherit the design of the tooling that is being built by IHEP people to insert the new DC-IT. Those installation tooling specific to the CGEM-IT will be designed and built by INFN at Ferrara and Frascati.

## **8.1.2 CGEM-IT construction**

The Rohacell mechanical structures for the anode and cathode assembly will be produced in Ferrara, where the innovative technique for their construction has been developed. The CGEM-IT layers will be built assembling the Rohacell based anode, cathode and CGEM foils in Frascati. The GEM foils will be glued to a cylindrical support and then they will be assembled together with the help of molds constructed specifically with this aim. Frascati currently hosts few experts among its staff, and will host additional manpower from IHEP and other Institutions, that did participate to the construction of the KLOE-2 CGEM-IT; we expect an effective knowledge transfer to the people that will be involved in the construction of the BESIII CGEM-IT.

Once built, the three layers will be assembled to form the CGEM-IT, that must be extensively tested both before, in Frascati, and after its delivery to IHEP. The deployment, commissioning and maintenance for the first year of the CGEM-IT will offer an unique opportunity to spread the knowledge related to building and maintaining such unusually large-area CGEM detectors among the Collaboration in general and in particular among the IHEP personnel, that is likely to provide in the future most of the day by day support to the CGEM-IT, and will require quite extended stays at IHEP for personnel involved in Europe in the assembly and first tests of the detector.

The different sub-tasks of the current task are described herewith.

### 8.1.2.1 Production of the Rohacell structures (INFN)

Making use of Rohacell supports instead of the standard Honeycomb ones requires to develop full custom techniques in order to produce supports as thin as possible and yet with the required robustness.

These techniques have been developed in Ferrara and the construction of the supports for the middle layer is almost complete. The Rohacell supports for the inner and the outer layers will be built in Ferrara as well.

### 8.1.2.2 Assembly of the different components (Rohacell supports, cathode, CGEM foils and anode) to form CGEM-IT layers (INFN and IHEP)

The assembly of the different sub-layers to form each layer of the CGEM-IT will be performed by INFN staff with the supports of IHEP experts supported by IHEP within the INFN-MAE-MOST Project (see Sec. 8.4.2). Few of them will share their experience gained building the KLOE-2 CGEM-IT.

The BESIII CGEM-IT is in fact a new and innovative detector, even w.r.t. the KLOE-2 CGEM-IT, but it is quite safe to assume that those techniques needed to assemble the sub layers will be quite close to the ones developed by KLOE-2 experts when their CGEM-IT has been built.

Since the procurement of the needed material is basically complete, the assembly of the middle layer will start in Frascati in September 2014.

### 8.1.2.3 Assembly of the three layers in one single CGEM-IT (INFN and IHEP)

The three layers will be assembled in Frascati, completing what started in the previous sub-task, within the first half of 2016. A possible alternative option could be to deliver the single layers unassembled to IHEP, for a safer dispatch, and to proceed to the assembly directly in IHEP.

### 8.1.2.4 Test of the CGEM-IT before its delivery to IHEP (INFN and IHEP)

The assembled layers will be tested in Frascati making use of temporary electronics, before dispatching the CGEM-IT to IHEP.

### 8.1.2.5 Deployment of the CGEM-IT in IHEP (INFN and IHEP)

Once the BESIII CGEM-IT will be delivered to IHEP, the final FEE electronics will be installed, and the HV and the slow control systems connected. The crucial and most challenging step of this sub-task is the insertion of the CGEM-IT into the BESIII Outer DC. Extended stays of staff from INFN, Mainz and Uppsala is needed, in tight cooperation with IHEP people and in particular with those that will have in the meantime developed the proper procedure to insert the new DC-IT in the Outer DC.

### 8.1.2.6 Commissioning of the CGEM-IT (INFN and IHEP)

The commissioning of the CGEM-IT, once the deployment is complete, will last at least until the end of 2018. Several aspects, related to mechanics, electronics, simulations and data analysis will have to be considered when commissioning the CGEM-IT; this task is hence closely interconnected with those described in Sec. 8.1.3 for the following task. Also in this case extended stays at IHEP for staff from INFN, Mainz and Uppsala will be necessary.

### 8.1.2.7 Maintenance of the IT in the first operational year (INFN and IHEP)

Once the CGEM-IT will have been commissioned, the proper procedures needed to its maintenance will be defined and then implemented; at least for the full 2018 this will be a sub-task shared among INFN and IHEP staff. A complete transfer to IHEP experts of all the aspects related to the commissioning and to the procedures needed to maintain the CGEM-IT must occur, in order to ensure a long term support to the CGEM-IT during the next years of data taking.

## 8.1.3 CGEM-IT electronics

The readout electronics developed for KLOE-2 does not fit the requirements of the BESIII CGEM-IT, because it provides only a digital information hit/no hit strip, while the CGEM-IT needs also the information about the charge centroid which allows to achieve the required spatial resolution of 100  $\mu\text{m}$ . Moreover, the GASTONE ASIC for KLOE-2 has been developed using AMS CMOS 0.35  $\mu\text{m}$  technology, which cannot be exported in P.R.C.. Hence, a new analogue readout must be designed in order to measure the charge centroid and to make over to a

different technology, such as UMC 0.11  $\mu\text{m}$ , which can be exported in P.R.C..

Full custom front end readout electronics and a state of the art ASIC will be developed in Turin in cooperation with Frascati; a significant contribution will also be offered by IHEP staff experts that will join the Microelectronics Laboratory in Turin to take part to the ASIC design and test. Such experts will be supported by IHEP within the INFN-MAE-MOST Project (see Sec. 8.4.2). The design and commissioning of the readout electronics will be supported by those Uppsala and INFN people that participated to the design and commissioning of the readout electronics of the KLOE-2 CGEM-IT.

The BESIII CGEM-IT HV system and the corresponding slow control must be designed as well and will be produced by Mainz in cooperation with Frascati.

The assembly and commissioning of the electronics in IHEP will offer an unique opportunity to transfer the relative knowledge to the IHEP personnel, that will likely provide in the future most of the day by day support to the CGEM-IT electronics.

#### **8.1.3.1 Development and implementation of a new ASIC for the analogue readout of a CGEM detector (INFN)**

A new ASIC suitable for the BESIII CGEM-IT readout according to the requirements described above will be developed in the INFN Microelectronics Laboratory of Turin. A PhD student has already joined INFN staff in January 2014, his grant being funded directly by IHEP, and will work on this task until the end of 2016. Two more experts from IHEP staff, an expert in analog ASIC design and an expert in FPGA programming and testing, will join the Microelectronics in Turin, for 12 months each, in order to allow for a first foundry run for a first prototype of the ASIC at the end of 2015, and for a final foundry to be completed within the end of 2016, providing the final ASICs for the readout of the CGEM-IT.

#### **8.1.3.2 Design and implementation of the board hosting the ASIC for the CGEM-IT (INFN)**

The board will be designed by Turin. A proper interfacing with the global readout system of BESIII must be granted.

#### **8.1.3.3 Development and implementation of the Front End readout electronics of the CGEM-IT (Uppsala and INFN)**

The same experts who were involved in the design and construction of the Front End readout electronics for the KLOE-2 CGEM-IT, cooperating with the same people from Frascati involved now in this project, will focus on this sub-task in order to design a similar electronics for the BESIII CGEM-IT.

#### **8.1.3.4 Development and implementation of the CGEM-IT HV system (Mainz and INFN)**

The HV system will be designed and built in Mainz profiting of the knowledge transfer from those Frascati experts who were involved in the design and construction of the HV system for the KLOE-2 CGEM-IT HV system. Most of the corresponding activities will be performed in 2016.

#### **8.1.3.5 Design of the CGEM-IT slow control system (Mainz)**

Mainz staff will focus on designing a proper slow control system for the CGEM-IT, matching and interfacing with the existing BESIII slow control system, within 2016.

#### **8.1.3.6 Assembly of the electronics once the CGEM-IT has been deployed in IHEP (INFN, IHEP and Uppsala)**

All the final electronics will have to be installed on the CGEM-IT: the readout boards hosting the ASIC developed by INFN, the Front End electronics developed by Uppsala and INFN, the HV and slow control systems developed by Mainz. All the readout chain will have also to be interfaced with the existing systems of the BESIII spectrometer. Starting from the beginning of 2017 Mainz people will take care of the deployment of the HV system, while in the same period Frascati, Turin and Mainz people will provide general support for the deploying and commissioning of all the electronics.

#### **8.1.3.7 Integration of the CGEM-IT HV system with the global BESIII HV system (Mainz)**

The HV system has to be properly integrated with the existing BESIII HV system during the deploy-

ment at IHEP of the CGEM-IT. Mainz people will focus on this sub-task.

#### **8.1.3.8 Commissioning of all the CGEM-IT electronics in IHEP (INFN, Mainz, Uppsala and IHEP)**

The electronics, the readout chain, the HV and slow control systems must be commissioned, without and with regular beams, and both during specific tests or the regular data taking. Most of the people from INFN, Mainz and Uppsala involved in the CGEM-IT electronics will focus in 2017 on this sub-task together with IHEP people.

### **8.1.4 CGEM-IT data simulation and analysis**

Building the CGEM-IT is only part of the challenge; for the commissioning itself and a fruitful use in the future, significant efforts must be spent on the software side. A correct description of the CGEM-IT must be included in the simulation and reconstruction framework of the BESIII Collaboration, BOSS; proper algorithms to simulate the CGEMs signals and backgrounds, and to perform the tracking have to be developed and tested; the best benchmark channels have to be identified and investigated in order to define the improved capabilities of a BESIII spectrometer hosting the CGEM-IT.

In the next future a proper coordination with the BESIII Working Groups is needed in order to investigate how the current analyses may be improved by the availability of the CGEM-IT and which new analyses may eventually become accessible due to its performance.

#### **8.1.4.1 Description of the CGEM-IT in the BOSS framework (INFN, IHEP)**

A geometry reflecting the mechanical design and the material composition of the CGEM-IT must be created and maintained in GEANT4 in order to let the simulation and reconstruction software of BESIII, BOSS, to simulate and reconstruct data for a BESIII spectrometer hosting the CGEM-IT. This sub-task is already almost completed, thanks to the efforts of the involved IHEP people.

#### **8.1.4.2 Development of proper algorithms for reconstruction and tracking with CGEM-IT (INFN, IHEP and Mainz)**

The current Inner Tracker is a DC. The new Inner Tracker will be based on CGEM, characterised by a new strip readout on the anode, and an analogue readout approach that has not been used before. Usually GEM detectors are of smaller size and planar. Finally, the tracks from the CGEM-IT have to be bridged to an Outer DC. The tracking scenario is quite unique and requires the development of proper tracking algorithms optimised for this specific experimental scenario. Most of the manpower needed for this sub-task is and will be provided by IHEP, in continuous interaction with INFN people; Mainz should also soon provide an effective support to these developing activities.

#### **8.1.4.3 Knowledge transfer among experts and less experienced researchers of the different institutions for simulation and reconstruction (IHEP, INFN and Mainz)**

A significant contribution to data simulation and analysis, necessary for the commissioning of the detector first and for the optimisation of the future use of the CGEM-IT data later, should come from European researchers as well. Younger researchers should spend as much time as the funding of the project will be able to support in IHEP, creating an international software pool in IHEP in order to increase their capabilities in data simulation and analysis and get acquainted with BOSS. Quite long stays in IHEP must hence be foreseen starting already from 2015.

#### **8.1.4.4 Identify and investigate specific benchmark channels (INFN, IHEP and Mainz)**

Proper benchmark channels suitable to foresee and verify those improvements in tracking and event selection that can be introduced in BOSS making use of hits information from the CGEM-IT, must be defined and investigated, also in order to commission the CGEM-IT and to maximise the long term outcome of its construction. A common effort shared by INFN, IHEP and Mainz people.

#### 8.1.4.5 Analysis and validation of the CGEM-IT data (INFN, Mainz and IHEP)

The commissioning of the CGEM-IT can start from a first look at the data collected by the new detector; but people from INFN, Mainz and IHEP is expected then to provide a continuous analysis task force in order to support the commissioning activities for as long as it is needed. The goal is to commission the CGEM-IT within the end of 2017.

#### 8.1.4.6 Analysis of the CGEM-IT data: benchmark channels (Mainz and INFN)

A commissioned detector is only the starting point: a full investigation of the benchmark channels will finally start in order to validate the data simulation and analysis software related to CGEM-IT. This sub-task will be performed mostly by people from Mainz and INFN.

### 8.1.5 CGEM-IT DAQ and Trigger

The DAQ for the CGEM-IT is currently undefined. Manifestation of interest have come from the group of Giessen, that is applying for funds to support the related hardware and most of all the needed manpower. In case of success in such an application Giessen could cooperate with the DAQ and Trigger group in IHEP to provide what is needed for the CGEM-IT.

In case such application would be unsuccessful, to define who will develop and provide what is needed for this task would be an open issue to be very very soon addressed by the Collaboration, since the staff in IHEP is probably lacking the needed manpower. Either the group in IHEP could obtain some help, either additional contribution from other Institutions within the Collaboration should be searched for.

Some more work is also needed in order to include the CGEM-IT in the BESIII Trigger system, and to explore a possible Second-Level Trigger. Both this latter activities can be probably be effectively performed only by IHEP people already acquainted with the BESIII Trigger.

## 8.2 Schedule

The schedule currently foreseen for the hardware related tasks described above is reported in Fig. 8.1.

The main goals are:

1. to finalise the construction and the assembly of the CGEM-IT (without the final electronics) in Frascati within the end of 2016;
2. to deliver frontend electronics by the end of 2016;
3. to deliver to IHEP and deploy the assembled CGEM-IT at the beginning of 2017;
4. to be on the floor and to assemble the final electronics during 2017 in IHEP;
5. to conclude the commissioning of the detector within the end of 2017.

The year 2018 could hence be the first year of BE-SIII data taking effectively including the CGEM-IT information, and a proper tuning of the software and of the data analyses and simulations could be performed within 2018.

## 8.3 Manpower

The groups involved within the BESIII Collaboration in the CGEM-IT activities are composed of quite a large number of younger and more experienced researchers. Moreover practically all the Institutions quoted above may gain support for these activities from their home laboratories common support services for mechanics and electronics. We consider the available manpower suitable for the tasks that must be performed, with the only exception (for the time being, waiting for the success of the application of the Giessen group) of the CGEM-IT DAQ and Trigger.

Besides their components, people in Frascati and in Turin may count on additional manpower coming from IHEP for activities related to the CGEM-IT construction and assembly and to the ASIC design and testing; such manpower is funded by IHEP within the INFN-MAE-MOST Project (see Sec. 8.4.2).

A PhD student joined the Doctoral School of the Politecnico of Torino within an agreement with INFN that let him join the INFN ASIC development team in Turin, and two more students will come in the next two years. These three PhD positions are funded as well directly by IHEP.

**Figure 8.1:** Schedule currently foreseen for the hardware related tasks described in Sec. 8.1. Darker regions correspond to what has already been achieved.

## **8.4 Financial issues**

### **8.4.1 Direct Funding**

### **8.4.2 Indirect Funding**

**Figure 8.2:** Contributions in kind to the funding of the CGEM-IT construction and installation already secured: red, INFN-MAE-MOST indirect funds; or booked: light blue, INFN; green: HIM and Mainz University; orange: Uppsala University; blue: IHEP funds.



## Acknowledgments

We acknowledge the invaluable support of the KLOE-2 LNF team and in particular of Giovanni Bencivenni, Erika De Lucia, Danilo Domenici, and Gianfranco Morello that gave birth to a new kind of detectors: the Cylindrical-GEM based Inner Trackers.

We acknowledge financial support from:

- CSN1 - INFN - ITALY, and in particular Prof. Franco Bedeschi (Chairman of the INFN CSN1), Prof. Walter Bonivento, Prof. Franco Polesello and Prof. Franco Simonetto (BESIII Referees within the INFN CSN1);
- the Executive Board of INFN, and in particular Prof. Ferdinando Ferroni (INFN President) and Prof. Antonio Zoccoli (INFN Vice-President);
- IHEP, and in particular Prof. Yifang Wang (IHEP Director) and Prof. Xiaoyan Shen (BESIII Spokesperson);
- MAE - Italy and MOST - P.R.C. within the Executive Programme for Scientific and Technological Cooperation between the Italian Republic and the People's Republic of China for the years 2013-2015.



# Acronyms

---

<b>2eSST</b> Double-edged Structured Stream Transport	<b>EC</b> European Commission
<b>2eVME</b> Double-edged VME	<b>ENC</b> Equivalent Noise Charge
<b>3D</b> 3-Dimensional	<b>ENOB</b> Effective Number Of Bits
<b>ADC</b> Analog to Digital Converter	<b>EST-DEM</b> Design and manufacture of Electronic Modules (DEM) group of the Engineering Support and Technology division (EST)
<b>AMS</b> AustriaMicroSystems	<b>FEE</b> Front-End Electronics
<b>APV25</b> Analogue Pipeline chip, Voltage-mode, 0.25 micrometer technology	<b>FIFO</b> First In, First Out
<b>ASCII</b> American Standard Code for Information Interchange	<b>FPGA</b> Field-Programmable Gate Array
<b>ASIC</b> Application Specific Integrated Circuit	<b>GCL</b> Global Control Layer
<b>ATLB</b> Advanced Trigger Logic Board	<b>GEM</b> Gas Electron Multipliers
<b>BEPCII</b> Beijing Electro-Positron Collider II	<b>HIM</b> Helmholtz-Institut Mainz
<b>BESIII</b> BEIjing Spectrometer III	<b>HPTDC</b> High Performance TDC
<b>BLT</b> Block Transfer	<b>HV</b> High Voltage
<b>BOSS</b> BESIII Offline Software System	<b>ID</b> Identification
<b>CGEM</b> Cylindrical Gas Electron Multipliers	<b>IEEE</b> Institute of Electrical and Electronics Engineers
<b>CGEM-IT</b> CGEM - Inner Tracker	<b>IHEP</b> Institute for High Energy Physics - P.R.C.
<b>CMOS</b> Complementary Metal-Oxide Semiconductor	<b>INFN</b> Istituto Nazionale di Fisica Nucleare - Italy
<b>COMPASS</b> Common Muon and Proton Apparatus for Structure and Spectroscopy	<b>INL</b> Integral Non Linearity
<b>CSN1</b> Commissione Scientifica Nazionale 1 - INFN	<b>IT</b> Inner Tracker
<b>DAFNE</b> Double Annular Factory for Nice Experiments	<b>IP</b> Intellectual Property
<b>DAC</b> Digital to Analog Converter	<b>KLOE-2</b> K LOng Experiment, to study CP violation at LNF's DAFNE
<b>DAQ</b> Data Acquisition	<b>L1</b> Level 1
<b>DC</b> Drift Chamber	<b>LHCb</b> Large Hadron Collider beauty
<b>DC-IT</b> Drift Chamber - Inner Tracker	<b>LNF</b> Laboratori Nazionali di Frascati - Italy
<b>DC-OT</b> Drift Chamber - Outer Tracker	<b>LSB</b> Least Significant Bit
<b>DCS</b> Detector Control System	<b>LVDS</b> Low Voltage Differential Signaling
<b>DDR</b> Double Data Rate	<b>MAE</b> Ministero degli Affari Esteri - Italy
<b>DNL</b> Differential Non Linearity	<b>MBLT</b> Multiplexed Block Transfer
	<b>MDC</b> Main Drift Chamber
	<b>m.i.p.</b> minimum ionizing particle

**MOST** Ministry of Science and Technology -  
P.R.C.

**NIM** Nuclear Instrument Module

**PM** Photo Multiplier

**PMI** Polimetacrilimide

**P.R.C.** People's Republic of China

**PVC** Polyvinyl Chloride

**RAM** Random Access Memory

**r.m.s.** Root mean square

**ROM** Read Only Memory

**RISE** Research and Innovation Staff Exchange

**SEU** Single Event Upset

**SFO** Sub-Farm Output

**SFP** Small Form-factor Pluggable

**TDC** Time to Digital Converter

**ToT** Time-over-Threshold

**UMC** United Microelectronics Corporation

**USB** Universal Serial Bus

**VME** Versa Module Eurocard

**VXS** VMEBus Switched Serial

# List of Figures

---

1.1	MDC gain changes in each year (the up is from Bhabha events, and the down is from accumulated charges with aging ration of 0.3% methods).	2	3.1	Cross section of a portion of the interaction region of BES-III instrumented with CGEM-IT. . . . .	14
1.2	Spatial resolution (up) and hit efficiency (down) of each layer. . . . .	3	3.2	Drawing of the layer 2 CGEM showing the frontend cards located on the anode Permaglass ring. . . . .	14
1.3	The accumulated charges of MDC in each year. . . . .	3	3.3	3D model of a cylindrical GEM foil with the Permaglass rings at the edges.	15
1.4	The counting rate of each MDC layer, extracted processing the first 30 s of random trigger data. Top plot represents a run from 2012 and bottom plot is a run from 2014. . . . .	3	3.4	Lateral section of the Layer 2 showing the Permaglass rings acting as spacers between the electrodes. . . . .	15
1.5	Average rate per wire on the inner drift chamber as function of the radius, calculated with background mixing procedure as described in the text. Each point represents a layer. The inner drift chamber is composed by the first eight layers. Top plot represents a run from 2012 and bottom plot is a run from 2014. . . . .	4	3.5	Top: machining of the Rohacell during the fake cathode construction. Bottom: a picture of the fake cathode with the radius of the innermost layer of the CGEM-IT. . . . .	15
1.6	Average rate per wire on the first layer of the drift chamber for different running periods calculated with background mixing procedure. . . . .	4	3.6	One of the KLOE-2 complete GEM layers. BESIII GEM layers will be composed of only 2 GEM sheets, because of the BESIII CGEM-IT smaller radius. . . . .	17
1.7	Expected average rate per X-strip on the CGEM-IT as function the radius.	5	3.7	Two electrodes fixed on the vertical insertion system used to assembly the KLOE-2 detector. . . . .	18
2.1	Schematic of triple cylindrical GEM detector. . . . .	7	4.1	Dead time vs rate for different pile-up probabilities . . . . .	19
2.2	Left: the <i>jagged</i> layout where the overlap between the strips is reduced by decreasing the size of the X-strips on the intersections in order to minimize the inter-strip capacitance. Right: standard linear strip configuration. . . . .	8	4.2	CGEM IT front-end electronic chain block diagram . . . . .	20
2.3	Comparison of the capacitance between two single adjacent strips (top) and of X vs V strip (bottom) for prototype of different dimensions. . . . .	9	4.3	Cluster Charge Distribution (200 $\mu\text{m}$ pitch strips) without magnetic field . . . . .	20
2.4	The planar test setup in Frascati. . . . .	10	4.4	Cluster Charge Distribution with magnetic field and different gas gain (650 $\mu\text{m}$ pitch) . . . . .	20
2.5	Tracking resolution of the LNF cosmic setup. . . . .	11	4.5	Preamplifier support structure . . . . .	23
			4.6	Readout Board data flow architecture . . . . .	24
			4.7	VME64x ATLB . . . . .	24
			6.1	A side section of the CGEM-IT around the beam pipe. Only the layer 2 is designed with full level of details. . . . .	28
			6.2	HV segmentation to reduce GEM capacitance in case of discharge . . . . .	28

6.3	Single layer HV distribution block diagram . . . . .	29	8.1	Schedule currently foreseen for the hardware related tasks described in Sec. 8.1. Darker regions correspond to what has already been achieved. . .	43
6.4	High voltage distribution chain connection example . . . . .	29	8.2	Contributions in kind to the funding of the CGEM-IT construction and installation already secured: red, INFN-MAE-MOST indirect funds; or booked: light blue, INFN; green: HIM and Mainz University; orange: Uppsala University; blue: IHEP funds.	45
7.1	Diagram of digitization with (blue solid lines) and without (black dashed lines) taking into account the Lorentz angle $\alpha$ and electron diffusion. . . . .	31			
7.2	The flow diagram for the track reconstruction with CGEM-IT and DC-OT.	32			
7.3	The flow diagram for the preliminary track reconstruction with CGEM-IT and DC-OT. . . . .	32			
7.4	Schematic of one cluster induced by a charged track, composed of 3 X-strips and 4 V-strips on an unrolled CGEM plane, where the stereo angle $\alpha$ is the opening angle between X-strip and V-strip, the X axis is perpendicular to X-strips, the V axis is perpendicular to V-strips and the $\zeta$ axis is parallel to X-strips. . . . .	32			
7.5	The position residuals in X(top) and in V(bottom) of the cluster for a MC sample of single 1 GeV/c $\mu^-$ tracks.	33			
7.6	A schematic plot for illustrating a segment and an 8-wire group. The 4 layers of circles denote the signal wires in one super-layer. The arc shows a track, and the black solid circles are the fired wires of the particle. The 8 adjacent signal wires marked with a cross compose an 8-wire group used to match the segment pattern in segment finding. . . . .	33			
7.7	The ratio of the tracking efficiency with DC-OT only over the one with full MDC as a function of dip angle for barrel (left) and end-cap (right) Bhabha events. . . . .	34			
7.8	Ratio of the resolutions with which the secondary vertices corresponding to $\Lambda$ (red line) and $K_S^0$ (black line) charge mode decays are reconstructed by the DC-IT and the CGEM-IT. . . . .	35			

## List of Tables

---

3.1	Material budget calculation for the CGEM-IT cathodes. . . . .	16
3.2	Material budget calculation for the CGEM. . . . .	16
3.3	Material budget calculation for the CGEM-IT anodes. . . . .	16
4.1	Parameters used to estimate the achievable spatial resolution . . . . .	21
6.1	Number of HV macro-sectors/micro-sectors per layer and relative parasitic capacitance . . . . .	28
6.2	HV distribution system summary . . . . .	29